Environmental controls and phenology of sea ice algal growth in a future Arctic

Antoine Haddon, Patrick Farnole, Adam H. Monahan, Tessa Sou, and Nadja Steiner

2024

Original citation:

Haddon, A., Farnole, P., Monahan, A. H., Sou, T., & Steiner, N. (2024). Environmental controls and phenology of sea ice algal growth in a future Arctic. *Elementa: Science of the Anthropocene*, 12(1). https://doi.org/10.1525/elementa.2023.00129

ELEMENTA
Science of the Anthropocene

Haddon, A, et al. 2024. Environmental controls and phenology of sea ice algal growth in a future Arctic. *Elem Sci Anth*, 12: 1.
DOI: https://doi.org/10.1525/elementa.2023.00129

RESEARCH ARTICLE

Environmental controls and phenology of sea ice algal growth in a future Arctic

Antoine Haddon[1,*], Patrick Farnole[1], Adam H. Monahan[1], Tessa Sou[2], and Nadja Steiner[1,2,3]

The future of Arctic sea ice algae is examined using a regional ocean and sea ice biogeochemical model, with a simulation from 1980 to 2085, considering a future scenario with strong warming. To analyze the impacts of climate change, we computed key dates in the development of sympagic blooms, corresponding to the occurrence of specific growth conditions, and designed diagnostics of ice algal phenology to estimate the onset and peak of blooms. These diagnostics help understand how the timing of light and nutrient availability governs the growth of ice algae and how environmental controls will be altered by climate change across regions. With thinner ice, photosynthetically active radiation in bottom ice will reach levels sufficient for growth earlier, resulting in a better synchrony of high levels of light and nutrients. Increases in snow cover can potentially offset the effect of thinner ice, leading to shorter periods of favorable growth conditions in certain regions. The loss of sea ice cover before the late 21st century only impacts sympagic blooms at lower latitudes, as the timing of sea ice break-up shows little change relative to other key dates at higher latitudes. In response to climate change, the model simulates a modified spatial distribution of blooms, with the emergence of highly productive areas and the loss of blooms in other regions. However, the changes in the timing of growth conditions do not substantially alter the timing of blooms, and both onset and peak ice algae see little change. The simulated lack of sensitivity of bloom onset is attributed to the delay in sea ice freeze-up projected by the model, causing a reduction of overwintering ice algae. The resulting lower initial biomass at the beginning of spring then causes a delay in the development of blooms, offsetting earlier light from thinner ice.

Keywords: Ice algae, Arctic, Model, Future

1. Introduction

The Arctic Ocean includes diverse regions and a range of different sea ice environments, varying in ice and snow thickness, length of ice covered season, ice velocity and brine chemical composition (Petrich and Eicken, 2017). The microorganisms that colonize sea ice therefore experience a variety of different conditions, affecting their growth rate and the timing of the algal bloom that develops during spring. As a result, primary production and ice algal standing stocks are highly variable throughout the Arctic and the links between biomass variability and regional environmental conditions remain unclear (Lannuzel et al., 2020; Campbell et al., 2022b). Adding to these complexities, climate change impacts the Arctic strongly, with the current important and rapid modifications of the sea ice environment set to continue during the 21st century (Stroeve et al., 2012; Crawford et al., 2021). In particular, to improve projections of future change, the factors controlling the onset of blooms during the winter-spring transition and the relative importance of light and nutrients during the main growth phase still need to be better understood (Leu et al., 2015).

Satellite remote sensing of ice algal blooms at large scales remains impossible, and therefore models are currently the only option available to study the pan-Arctic distribution of ice algae. Since the introduction of the first three-dimensional (3D) ocean and sea ice models including ice algae, substantial spatial variability of sympagic blooms has been noted. Differences in sea ice dynamics and the duration of sea ice cover have been proposed to explain spatial patterns of sympagic growth (Sibert et al., 2010; Deal et al., 2011). Models have been used to explore the links between ice algal phenology and environmental timing (Ji et al., 2013), suggesting that bloom onset is controlled by the timing of light and termination by sea ice break-up (Sibert et al., 2010; Castellani et al., 2017). In

[1] School of Earth and Ocean Sciences, University of Victoria, Victoria, BC, Canada
[2] Fisheries and Oceans Canada, Institute of Ocean Sciences, Sidney, BC, Canada
[3] Canadian Center for Climate Modelling and Analysis, Environment and Climate Change Canada, Victoria, BC, Canada

* Corresponding author:
Email: ahaddon@uvic.ca

addition, models have shown that nutrients play a primary role in controlling primary production and the distribution of ice algae (Jeffery et al., 2020). By representing the various elements impacting ice algae, models can also help to investigate how a combination of environmental conditions drives bloom variability, such as the impact of wind patterns on nutrient supply through turbulent mixing (Watanabe et al., 2015).

Recently, an inter-comparison of five ice algal models confirmed that strong regional differences exist in Arctic sea ice blooms (Watanabe et al., 2019). No agreement was found among models on the total annual ice primary production, and different trends over 1980–2009 in bloom timing were simulated. Nonetheless, on average, the models suggest an earlier start and shorter blooms due to sea ice loss. However, almost all regional or pan-Arctic modeling studies have focused on the historical period. Only Tedesco et al. (2019) have presented spatially distributed simulations of future ice algae, albeit limited to zonally averaged projections. Using sea ice output from global climate models to drive a sea ice biogeochemical model, they found an overall increase of pan-Arctic gross primary production, with future ice algal blooms starting and ending earlier.

Here, we present the first pan-Arctic simulation of future ice algae from a coupled 3D ocean and sea ice biogeochemical model, analyzing the environmental drivers of spatial variability and how ice algae are impacted by climate change. We investigate the drivers influencing the distribution and timing of ice algal blooms and specifically, the relative importance of light and nutrients in controlling sympagic growth. To support the analysis, diagnostics are constructed to identify key dates in the development of ice algal blooms. These diagnostics are then used to assess how climate change affects sympagic ecosystems across regions, and to explain how physical changes affect the evolution of light and nutrient availability as well as timing. Finally, we address the issue of ice algal phenology and examine what controls the timing of sympagic blooms in a warmer Arctic.

2. Methods

2.1. Model

The regional model of the Arctic Ocean used in this study couples a 3D physical ocean model (NEMO 3.4; Madec et al., 2017) with a three-layer (one for snow and two for ice) dynamic-thermodynamic sea ice model (LIM2; Bouillon et al., 2009). The model includes the Canadian Ocean Ecosystem Model (CanOE; Christian et al., 2022), with iron limitation removed as it is not relevant to Arctic primary production. In addition, the model contains a sea ice biogeochemistry component, the Canadian Sea Ice Biogeochemistry model (CSIB; Hayashida et al., 2019), which considers a three-compartment sea-ice ecosystem (ice algae, nitrate, and ammonium) and a two component sulfur cycle. In addition to biological and chemical sources and sinks, the model simulates the horizontal transport of biogeochemical state variables within sea ice and is coupled to the pelagic ecosystem through exchanges at the sea ice–ocean interface by diffusion, ice growth or melt, and freshwater flushing.

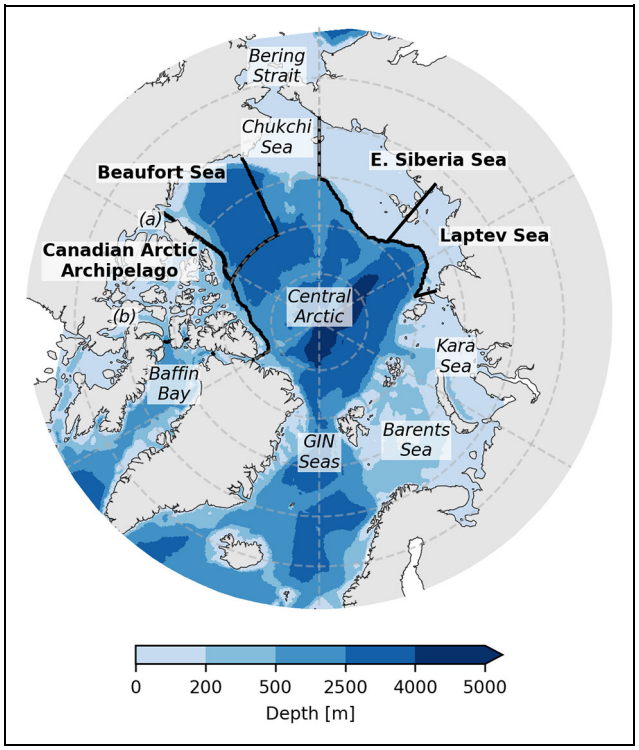

Figure 1. Map of the Arctic Ocean. Regions with bold names are those used in later figures. GIN indicates Greenland, Iceland, and Norwegian seas; (a) Amundsen Gulf; (b) Gulf of Boothia.

The sea ice biogeochemical model was first developed in the context of a 1D model and evaluated with observations (Hayashida et al., 2017; Mortenson et al., 2017). This model was then integrated in a 3D model of the Arctic (Hayashida et al., 2019) and further evaluated for the historical period in Hayashida et al. (2020) and in Mortenson et al. (2020). The model configuration used here corresponds to the one used in Hayashida et al. (2020).

The spatial domain (**Figure 1**) covers the entire Arctic, north of approximately 60°N, the Bering Strait and the northern North Atlantic, with a horizontal resolution ranging from 10 km to 14.5 km and 46 vertical ocean layers.

2.1.1. Ice algae

The CSIB model only considers ice algae that grow on the bottom of the ice in the skeletal layer, with sympagic growth limited by the availability of photosynthetically active radiation (PAR) and nitrogen (N), as well as ice growth or melt. The growth rate depends on non-dimensional limitation factors (L_N, L_{PAR}), ranging between 0 and 1, with 0 representing total growth limitation and 1 unlimited growth (**Figure 2**). The growth rate μ_{IA} depends on the minimum of the limitation factors:

$$\mu_{IA} = \mu_{\max}\, f(T)\min(L_N, L_{PAR})IA \qquad (1)$$

with IA the ice algal concentration (mmol C m^{-3}). The growth rate also depends on the temperature T, which is

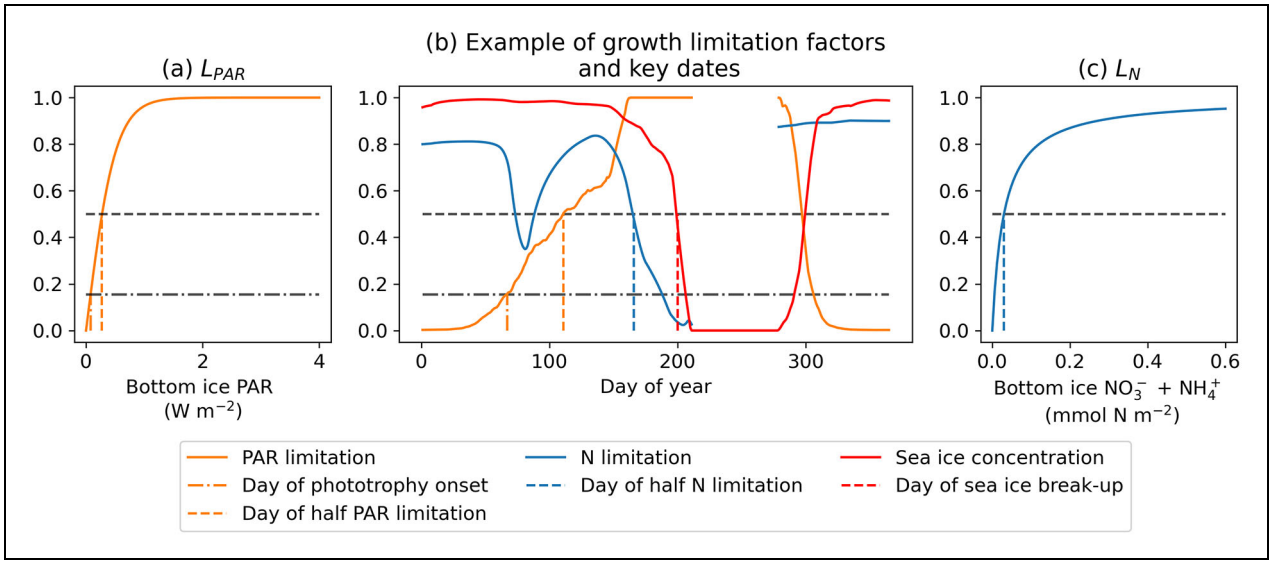

Figure 2. Limitation factors used in ice algal growth rate computation and example of key dates. (a) Light limitation factor L_{PAR} as a function of bottom ice photosynthetic active radiation (PAR). (b) Example, for one grid cell and one year, of key dates, growth limitation factors and sea ice concentration as functions of time. (c) Nitrogen (N) limitation factor L_N as a function of bottom ice $NO_3^- + NH_4^+$. Phototrophy onset corresponds to the first day bottom ice PAR reaches the lowest reported light compensation intensity. Half PAR limitation corresponds to the first day when L_{PAR} reaches 0.5 and half N limitation is the last day L_N is greater than 0.5. Sea ice break-up is defined as the first day the sea ice concentration reaches 50%.

Table 1. Selected model parameters

Parameter	Value	Units	Description
k_N	1.0	mmol N m^{-3}	Nitrogen half-saturation constant
$\frac{C}{N}$	8.83	(no units)	Carbon to nitrogen ratio
m_1	0.03	d^{-1}	Linear mortality parameter
m_2	0.00015	(mmol C m^{-3})$^{-1}$ d^{-1}	Quadratic mortality parameter
z_{IA}	3	cm	Skeletal layer thickness
$\frac{\alpha_{IA}}{P_{IA}}$	2.0	(W m^{-2})$^{-1}$	Ratio of photosynthetic parameters
$\mu_{\max}$	0.85	d^{-1}	Maximum specific growth rate
ε_{sn}	10.0	m^{-1}	Attenuation coefficient of snow
ε_i	1.5	m^{-1}	Attenuation coefficient of sea ice

generally at the freezing point in the skeletal layer of the ice. The light limitation factor is determined by the PAR reaching the bottom ice layer,

$$L_{PAR} = \tanh\left(\frac{\alpha_{IA}}{P_{IA}}[PAR]\right) \quad (2)$$

with tanh the hyperbolic tangent function, and α_{IA} and P_{IA} parameters representing respectively the photosynthetic efficiency and maximum photosynthetic rate. The nitrogen limitation factor depends on the nitrate NO_3^- and ammonium NH_4^+ concentrations,

$$L_N = \frac{[NO_3^-] + [NH_4^+]}{k_N + [NO_3^-] + [NH_4^+]} \quad (3)$$

with k_N the half-saturation constant for nitrogen.

The ice algal concentration is initiated during the formation of new ice from the uptake of phytoplankton, assuming that the ice algal concentration of newly formed ice is equal to the phytoplankton surface seawater concentration. The model considers linear and quadratic mortality terms, which are active only when the ice algal concentration is above 10 mmol C m^{-3} (corresponding to a skeletal layer biomass of 3.6 mg C m^{-2}) in order to maintain a reasonable overwintering biomass. Moreover, the model represents the horizontal transport of ice algae due to ice motion, and flushing of ice algae can occur due to the flow of water through the ice from rainfall and snow or ice melt. Details of these terms can be found in Mortenson et al. (2017) and Hayashida et al. (2019), and parameter values are presented in **Table 1**.

2.1.2. Simulations

Simulations of the recent past and of the future are analyzed here. For the historical run (1979–2015), surface and lateral boundary conditions are forced with the Drakkar Forcing Set (DFS, version 5.2; Dussin et al., 2016) and the Ocean Reanalysis System 4 (ORAS4; Balmaseda et al., 2013). Further details on the setup and initialization of the historical run can be found in Hayashida et al. (2019).

The future run (2016–2085) corresponds to the scenario Representative Concentration Pathway (RCP) RCP8.5 (van Vuuren et al., 2011), with atmospheric forcing from the Canadian Regional Climate Model (CanRCM4) for air temperature, humidity, total precipitation, snowfall, long wave, and short wave radiation. Because the CanRCM4 grid does not fully cover the simulation domain used here, data from the Canadian Earth System Model version 2 (CanESM2; Arora et al., 2011) were used to fill in the area not covered by the CanRCM4 data. Trends and projections in driving variables (near-surface temperature, wind speed, precipitation, and snowfall) from CanRCM4 have been evaluated and compared with other models by Reader and Steiner (2022). In this earlier study, trends were shown to agree favorably with those from observations. Lateral boundary conditions for the future run are restoration to output from CanESM2 (Arora et al., 2011) for ocean velocities, temperature, salinity, nitrate, alkalinity, and dissolved inorganic carbon. CanESM2 does not include ocean oxygen concentration; therefore, the lateral boundary condition is set from the difference between oxygen saturation concentration (computed from temperature and salinity) and nitrate concentration (Weiss, 1970; Owens and Millard, 1985). Other biogeochemical variables are fixed with the same constants used for the historical run (Hayashida et al., 2019).

In the future run, surface and lateral forcings from CanRCM4 or CanESM2 are adjusted to account for model biases. Future forcing daily time series F_{ANOM} are corrected by adding the anomaly between modelled and observed climatologies.

$$F_{ANOM} = C_{OBS} + (C^F_{SIM} - C^H_{SIM}) + (F_{SIM} - C^F_{SIM}) \quad (4)$$

The change between the historical C^H_{SIM} and future C^F_{SIM} simulated monthly climatologies (from CanRCM4 or CanESM2) is added to the observed historical monthly climatology (C_{OBS}, from DFS or ORAS4). The future simulated daily variability is retained by adding back the difference between the future daily time series F_{SIM} and the future monthly climatology. The historical climatology is computed over the period 1986–2005 and the future climatology over the period 2006–2085.

2.2. Diagnostics

To analyze the impact of environmental conditions on the phenology of ice algal growth, we compute from model output a number of key dates relevant in the development of sympagic blooms.

2.2.1. Day of phototrophy onset

The day of phototrophy onset estimates when growth from photosynthesis can begin. It is defined here as the first day in the year when bottom ice PAR reaches the lowest reported ice algal light compensation intensity, that is, when light is sufficient for the rate of photosynthesis to exceed the rate of respiration (orange dash-dot line in **Figure 2**). In this study, we identify the threshold bottom ice PAR as 0.079 W m^{-2}, which corresponds to 0.36 μmol photons m^{-2} s^{-1} as reported by Mock and Gradinger (1999), considering 4.6 μmol photons J^{-1} for PAR (Stroeve et al., 2021). This level of radiation is very low, such that growth remains light-limited for some time after the day of phototrophy onset.

2.2.2. Day of half PAR limitation

To characterize periods of high growth, we consider the days when growth limitation due to light or nutrients reaches a certain threshold. The day of half PAR limitation is defined as the first day each year that bottom ice PAR reaches the level corresponding to $L_{PAR} = 0.5$ (orange dashed line in **Figure 2**) and identifies when growth is no longer strongly limited by the lack of light. In this study, $L_{PAR} = 0.5$ corresponds to bottom ice PAR of 0.27 W m^{-2} (or 1.231 μmol photons m^{-2} s^{-1}). For reference, the day of phototrophy onset corresponds to a limitation factor of $L_{PAR} = 0.155$.

2.2.3. Day of half N limitation

The day of half N limitation is the last day the nitrogen concentration in the skeletal layer is above the level corresponding to $L_N = 0.5$ (blue dashed line in **Figure 2**). This diagnostic identifies when growth begins to be nutrient-limited, assuming nutrient-replete conditions in mid-winter. As nutrients in the ice can also be replenished from the ocean or locally through remineralization, changes in L_N can be non-monotonic; for the computation of this diagnostic, finding the last day during spring when $L_N \geq 0.5$ is important. In practice, difficulties in identifying this day arise when spikes in bottom ice N occur during sea ice break-up which may cause the N level to jump. To ensure consistency, we apply the following procedure: first, we identify the winter maximum as the day before September when the bottom ice N concentration is greatest, and then we find the first day after the winter maximum when $L_N \leq 0.5$. Next, we check whether L_N increases above 0.5 afterward and remains such for at least 5 days. If so, we identify the next day when $L_N \leq 0.5$, and if not we keep the first day found.

The choice of $L_{PAR} = 0.5$ and $L_N = 0.5$ as limitation thresholds is somewhat arbitrary. By construction, $L_N = 0.5$ corresponds to bottom ice N equal to the half-saturation constant k_N used in the definition of L_N (here 1 mmol N m^{-3}). Other limitation levels were tested, specifically L_{PAR} and $L_N = 0.4$ and 0.9 in both cases, but 0.5 yielded the clearest characterization of environmental controls of ice algal blooms. The definitions of these diagnostics are not always satisfied, and no value is returned where the PAR or N limitation factor is always below or always above the 0.5 threshold.

2.2.4. Day of sea ice break-up

The day of sea ice break-up is used here as a means to estimate when ice melt has become sufficient to trigger

the end of the bloom. It is defined as the first day after the winter maximum when the sea ice concentration is less than 50% (red dashed line in **Figure 2**), similarly to other studies (Crawford et al., 2021). In addition, we exclude areas where sea ice is either always present or never fully formed, defined respectively as the 30-day rolling mean sea ice concentration always above 50% (the perennial ice zone) or always below 50% (the marginal ice zone).

2.2.5. Day of bloom onset

To assess ice algal bloom phenology, the day of bloom onset is defined as the first day that ice algal biomass reaches the level of one standard deviation of the ice algal biomass calculated over the period from January 1 to August 31. Using the standard deviation as a reference to determine when ice algae reach a significant level was first proposed by Tedesco and Vichi (2014), arguing that a relative threshold is better suited to deal with the large variability of sea ice biomass in the Arctic.

2.2.6. Day of maximum ice algae

Finally, the day of maximum ice algae is computed as the day the maximum biomass is reached between January 1 and August 1. This day is indicative of the beginning of the bloom termination.

2.2.7. Phototrophic period

From the key dates of environmental timing, we define two growth periods. First, the phototrophic period is defined as the number of days from the day of onset of phototrophy to sea ice break-up or September 1, whichever is earlier. This quantity estimates the length of time during spring when growth from photosynthesis is possible.

2.2.8. High growth days

Next, the high growth days diagnostic is defined as the number of days from the day of half PAR limitation to half N limitation or sea ice break-up, whichever is earlier. If half N limitation occurs before half PAR limitation, then the number of high growth days is negative and characterizes the mismatch between the periods of light and nutrient availability. Conversely, when half N limitation occurs after half PAR limitation, this diagnostic represents the length of time when growth is the least limited.

2.2.9. Ice algal biomass

As indicators of ice algal blooms, we consider ice algal biomass. We choose not to use net primary production (NPP) as it accounts only for net growth whereas biomass accounts for all processes affecting ice algae, including transport. This latter process is particularly relevant for the termination of ice algal blooms, which are caused by brine flushing during ice melt, and thus is not accounted for directly in NPP. Both phenology diagnostics could be computed alternatively from ice algal net primary productivity. A comparison of phenology diagnostics computed from biomass and net primary productivity is presented in the supplementary material (Text S1, Figures S1, S2, and S3), and shows that overall the timing of bloom onset and peak computed from net primary productivity are similar to those computed from biomass.

At each grid cell, we compute the spring and fall biomass maxima, respectively, over the period from January 1 to August 31 and from September 1 to December 31. In addition, to estimate the initial biomass at the beginning of spring, we consider the ice algal biomass on the day of phototrophy onset.

2.2.10. Sea ice and snow thickness

To assess the relative impact of sea ice and snow on light availability timing, we compute the ice and snow thicknesses on the days of phototrophy onset and of half PAR limitation.

2.2.11. Diagnostics computation

All date diagnostics are computed from daily model output smoothed using a 14-day rolling mean. The smoothing is done to avoid problems in identifying wrong dates due to spurious spikes. For example, if sea ice concentration drops for only a few days during spring and then reforms, without this smoothing the computed sea ice break-up date would be identified too early. All diagnostics are computed for each grid cell and for each year, and are then averaged over 20-year periods to obtain climatological means.

In this work, three periods of analysis are considered. We define the recent past as the period 1981–2000, the near future as 2023–2042, and the late 21st century as 2066–2085. The late 21st century period defined here does not cover the end of the 21st century, and as a result our analysis does not consider the impacts of climate change beyond 2085, such as the acceleration of sea ice loss in the last decades of the 21st century, as projected by Earth system models participating in the Coupled Model Intercomparison Project (CMIP6; Crawford et al., 2021). The choice of 20-year periods could influence results due to multi-decadal variability. The trends analyzed in this work were checked with time series of regional means (not shown) to ensure that they are robust to the choice of 20-year period.

To illustrate the regional spatial distribution of diagnostics, histograms are presented. For this illustration, we use regions initially defined in Matrai et al. (2013) and shown in **Figure 1**.

2.3. Evaluation of sea ice break-up date

In addition to general model evaluations performed by Hayashida et al. (2020), we assess model performance in terms of the timing of environmental conditions by evaluating the timing of sea ice break-up with satellite remote sensing data. We use the daily sea ice concentration datasets AMSR-E ASI (version 5.4, June 2002 to September 2011; Spreen et al., 2008; Melsheimer and Spreen, 2020) and AMSR2 ASI (version 5.4, July 2012 to December 2019; Melsheimer and Spreen, 2019). We compute the day of sea ice break-up for each grid cell of both remote sensing and model data with the same methodology as described above, for 2003 to 2015, excluding 2002 and 2012 where observations are not

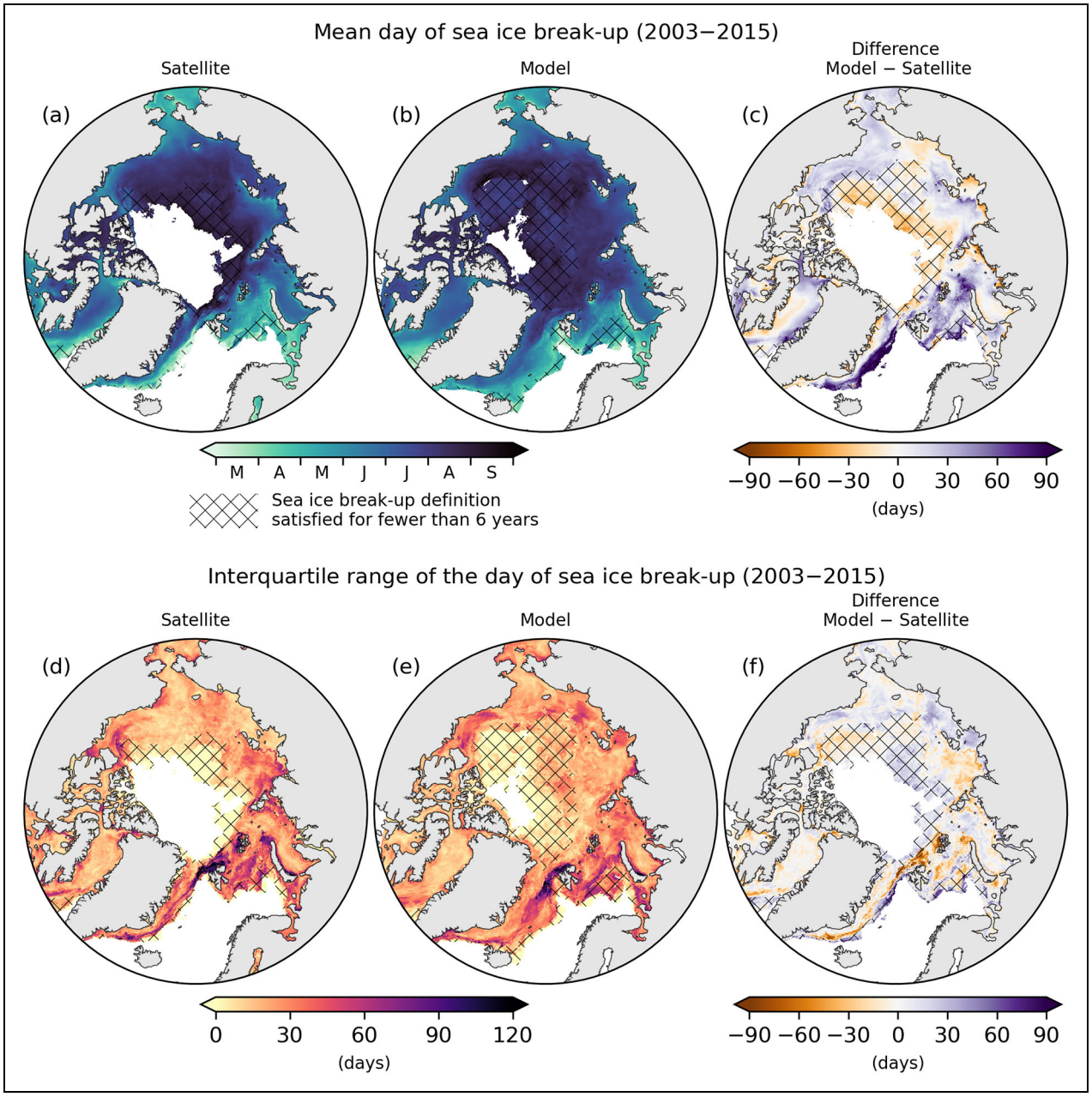

Figure 3. Evaluation of sea ice break-up timing. Mean day of sea ice break-up from (a) satellite remote sensing data and (b) model simulations, with (c) difference between observation and simulation. Interquartile range of the day of sea ice break-up for (d) satellite remote sensing data and (e) model simulations, with (f) differences between both. Data from 2003 to 2015, excluding 2012. Hatching indicates areas where the diagnostic definition is satisfied for less than 6 of 12 years for which statistics are less reliable. Sea ice break-up is defined as the first day the 14-day rolling mean sea ice concentration reaches 50%.

available for the entire year. The years 2016–2019 are not included as these years are driven by climate model projections rather than reanalyses based on historical observations. We consider temporal averages over the 12 years of commonly available data and compute the difference between observed and simulated means, by regridding model data to the finer remote sensing grid, using the xESMF package (Zhuang et al., 2023). Inter-annual variability is also evaluated by computing the interquartile range, defined as the difference between 75th and 25th percentiles of the data.

3. Results

3.1. Evaluation of sea ice break-up date

Comparing model and remote sensing climatologies of the day of sea ice break-up (**Figure 3a**, **b**) reveals that the model reproduces the large-scale spatial patterns of sea ice timing reasonably well throughout the Arctic. Similar gradients are resolved from the ice edge toward the interior and from the perennial to the seasonal ice zone, in both model and remote sensing. For example, on average, sea ice retreat begins in April in the Bering Strait, progressing north in the Chukchi Sea during late spring until it

reaches higher latitudes in September. However, mismatches due to spatial shifts of the patterns of break-up dates are evident (**Figure 3c**). In the Greenland, Iceland, and Norwegian (GIN) and Barents seas, the location of the ice edge is not resolved adequately, leading to errors of more than 2 months despite comparable large-scale gradients. Similarly, the model has difficulties simulating the precise size and location of the perennial ice zone in the central Arctic where our sea ice break-up definition is satisfied for fewer than 6 of the available 12 years of simulation.

Overall, the model simulates a later day of sea ice break-up than the remote sensing climatology. This delay could be linked in part to a bias in simulations toward larger maximal ice extent, with an ice edge at lower latitudes requiring more time for sea ice retreat to progress north and delaying the timing of sea ice break-up. Model timing of sea ice break-up is only earlier than observations in the central Arctic, and coastal areas, such as in the East Siberian and Laptev seas, as well as Baffin Bay.

The spatial patterns of inter-annual variability, estimated with the interquartile range, are also similar in remote sensing data and simulations (**Figure 3d**–**f**), further highlighting the model's ability to capture the large-scale spatial and temporal features of the Arctic sea ice environment. Notably, areas of strong inter-annual variability, such as the GIN and Barents seas, correspond to those showing the largest differences between observation and model sea ice break-up timing.

3.2. Growth conditions in the recent past (1981–2000)

We begin the presentation of these results by exploring the relations between environmental timing and ice algal growth during the recent past to provide context for future changes.

3.2.1. Phototrophic period

The day of phototrophy onset marks the beginning of light availability and generally occurs first in the series of key dates presented here (**Figures 4a** and **5a**). In the recent past, substantial spatial variability can be seen in this diagnostic, with a pan-Arctic range from January to July (Figure S4) and pronounced latitudinal gradients. The earliest onset of phototrophy takes place at lower latitudes but also notably in the Laptev Sea (**Figure 5a**). There are strong differences among the various regions of the Arctic: for instance, in the Canadian Arctic Archipelago (CAA) the onset of phototrophy is spread over five months (end of February to early July; **Figure 4m**), whereas in the East Siberian Sea it is concentrated within little more than a month (mid-April to end of May; **Figure 5m**).

Ice and snow thicknesses on the day of phototrophy onset (**Figure 6a** and **d**) reveal that in a large part of the Arctic, snow melt controls the timing of phototrophy onset. Indeed, in the central Arctic, Beaufort and East Siberian seas, sea ice is over 2 m thick on this day while the snow cover is reduced to less than 10 cm, indicating the necessity for snow to start melting before phototrophy can begin. However, at the high latitudes of the Barents Sea and in the Kara Sea, snow is substantially thicker and ice thinner than in the central Arctic, which suggests that ice is sufficiently thin for phototrophy to occur before snow melt. In areas where the day of phototrophy onset is the earliest, both ice and snow are thinner than in the rest of the Arctic, such as in the Laptev Sea, Baffin Bay, and the lower latitudes of the CAA.

Compared to phototrophy onset, there is much less variability in the day of sea ice break-up (**Figures 4d**, **m**, **p** and **5d**, **m**, **p**). In most of the high Arctic, sea ice break-up occurs over 2 months (July and August, Figure S5) and is earlier only at lower latitudes (Baffin Bay) or inflow seas (Barents Sea and Bering Strait). A large area in the central Arctic remains ice-covered year round and thus has more than 10 out of 20 years with no break-up date during the recent past period (hatched areas in **Figures 4d** and **5d**).

The phototrophic period (**Figure 7a**), counting the number of days when there is sufficient light for photosynthetic growth during spring, can be less than a month at lower latitudes where sea ice retreats early, such as the GIN and Barents seas, and at high latitudes in areas covered by the thickest ice, such as north of the CAA. In contrast, the phototrophic period can extend to more than 6 months in Baffin Bay or the Laptev Sea, where the onset of phototrophy is earlier than in the surrounding seas. Throughout the Arctic, the variability of the phototrophic period appears to be driven mainly by the spatial pattern of the day of phototrophy onset, as a consequence of the relative uniformity in the sea ice break-up date.

3.2.2. High growth days

The day of half PAR limitation (**Figures 4b** and **5b**) represents the point in time when growth is no longer strongly limited by light, and shares spatial variability and patterns similar to the day of phototrophy onset, including clear latitudinal gradients (Figure S6). Occurrence of half PAR limitation differs among regions and ranges from January to August in the recent past, with a spread of up to 5 months in the CAA (**Figure 4m**) and for the most part less than a month in the East Siberian Sea (**Figure 5m**). The lag from low to high light, that is, the time from phototrophy onset to half PAR limitation, also varies strongly across regions, from less than a month in the East Siberian Sea to nearly 2 months in the Laptev Sea (**Figure 5a**, **b**). Spatial patterns of ice and snow thicknesses (Figure S7) are similar to those on the day of phototrophy onset, such that at high latitudes half PAR limitation occurs after snow thickness is substantially reduced. In contrast, in the marginal ice zone at lower latitudes, sea ice is thinner, allowing a day of half PAR limitation despite a larger snow cover.

The day of half N limitation, marking the end of high nutrient availability, occurs from February to mid-June throughout the Arctic (**Figures 4c** and **5c**). As this diagnostic is the result of complex interactions between the physical and biological processes, its spatial patterns are considerably less straightforward to interpret than purely physical diagnostics. The day of half N limitation displays comparatively less variability than half PAR limitation, and

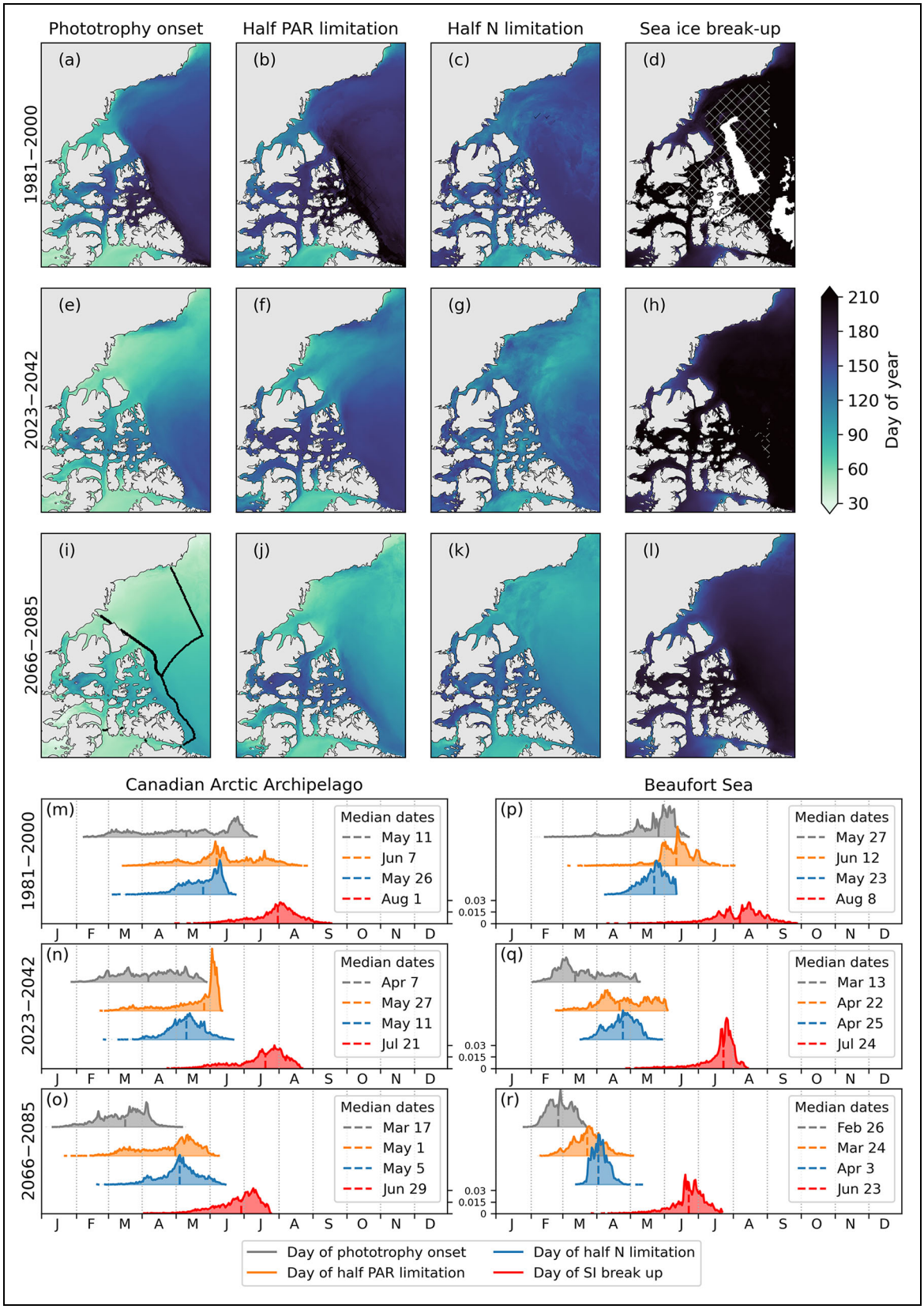

Figure 4. Key dates for the Canadian Arctic Archipelago and Beaufort Sea. (a–l) Regional maps of key dates and (m–r) corresponding spatial histograms showing the distribution of key dates for each region. The 20-year means are computed over recent past (a–d, m, p) 1981–2000, near future (e–h, n, q) 2023–2042, and late 21st century (i–l, o, r) 2066–2085. Hatching indicates areas where the diagnostic definition is satisfied for less than 10 out of 20 years. Diagnostics are described in Section 2.2.

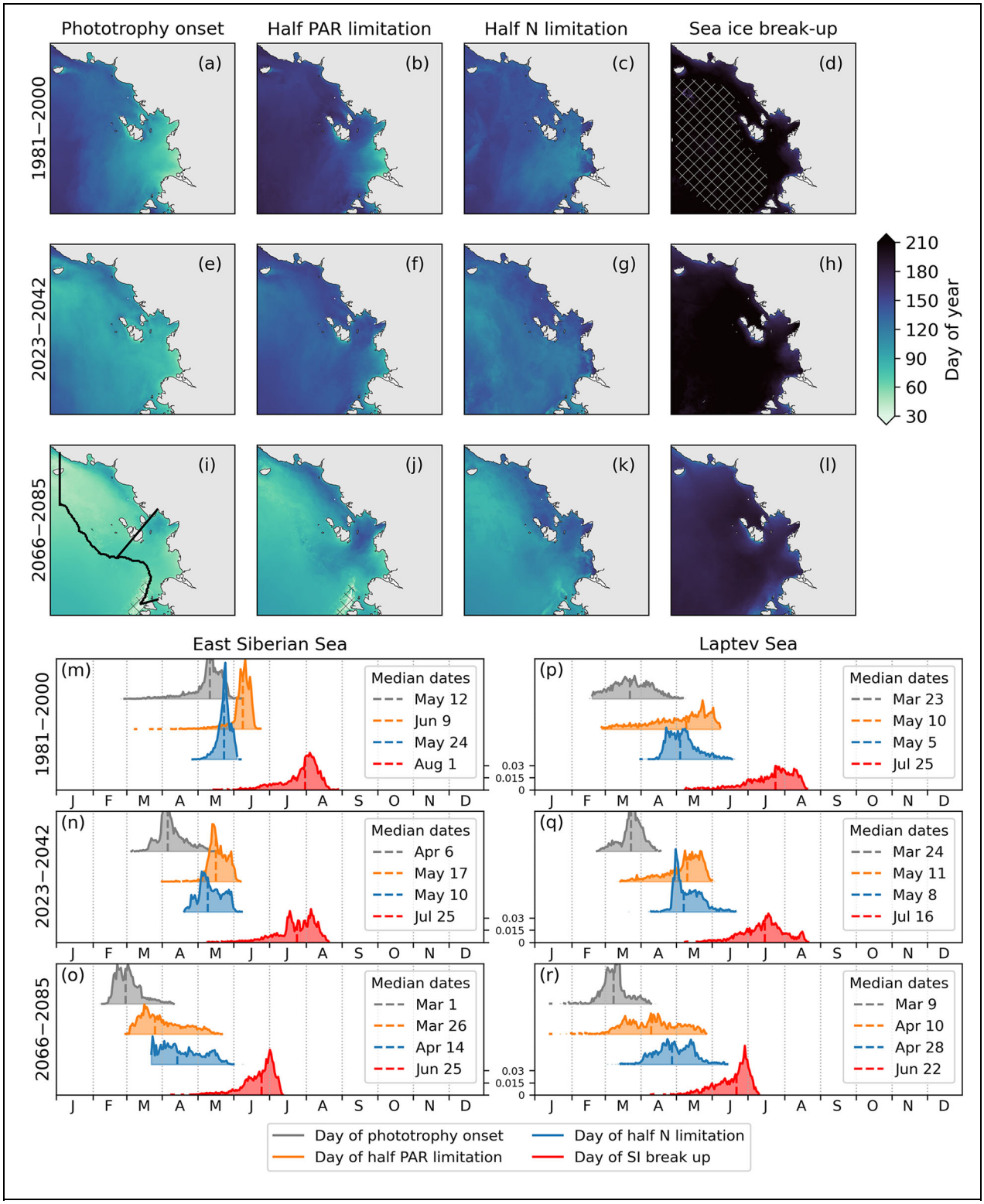

Figure 5. Key dates for the East Siberian and Laptev Seas. (a–l) Regional maps of key dates and (m–r) corresponding spatial histograms showing the distribution of key dates for each region. The 20-year means are computed over recent past (a–d, m, p) 1981–2000, near future (e–h, n, q) 2023–2042, and late 21st century (i–l, o, r) 2066–2085. Hatching indicates areas where the diagnostic definition is satisfied for less than 10 out of 20 years. Diagnostics are described in Section 2.2.

in the CAA, for example, it ranges over 2 months as opposed to 5 months for half PAR limitation (**Figure 4m**).

The number of high growth days (**Figure 7b**), counting from light to nutrient limitation, can be positive, if the day of half PAR limitation is first, or negative, if the day of half N limitation is first. In the recent past, over a large area ranging from the central Arctic to the peripheral seas, the number of high growth days ranges from

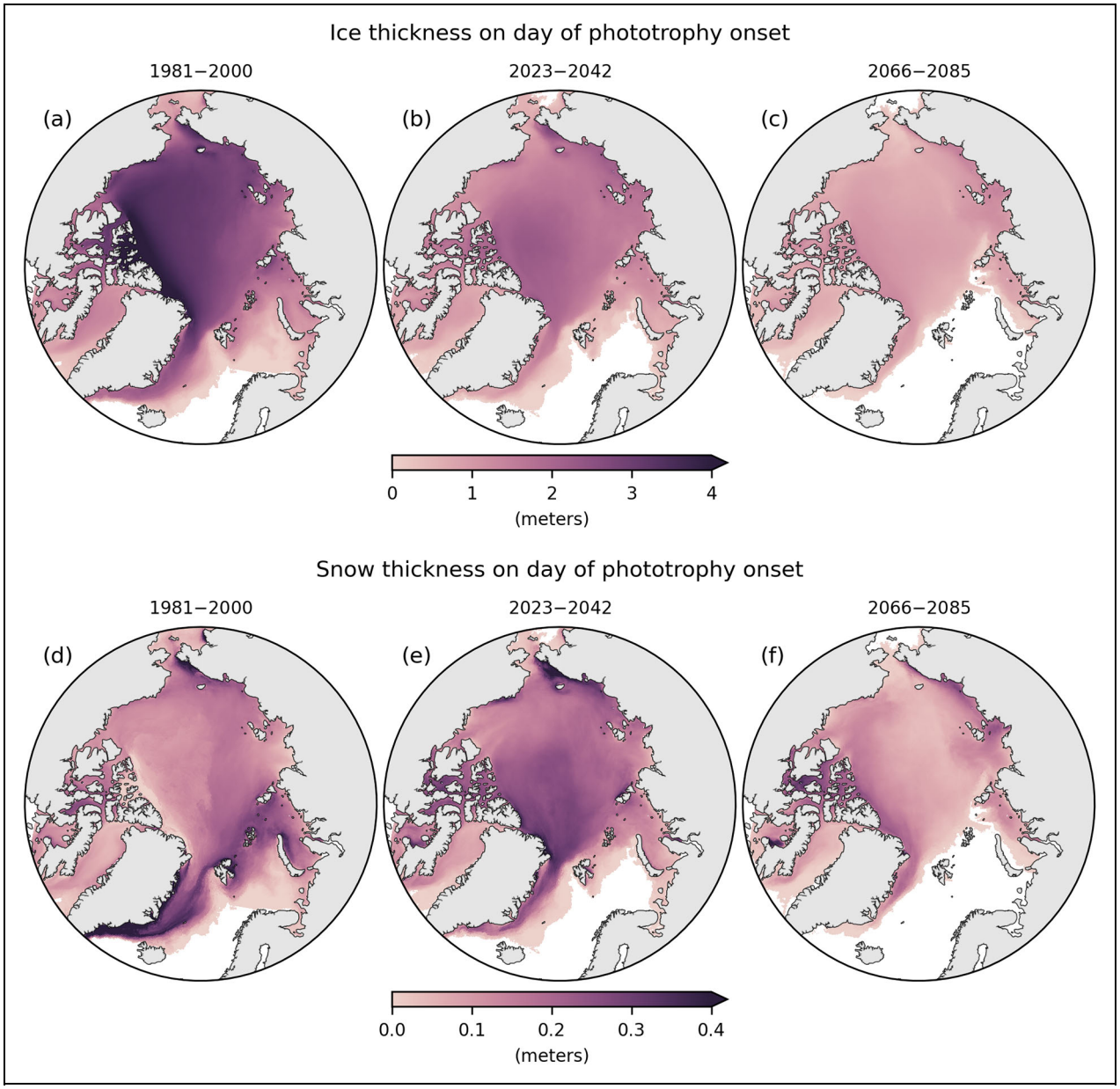

Figure 6. Ice and snow thickness on the day of phototrophy onset. Climatological (a–c) sea ice and (d–f) snow thickness on the day of phototrophy onset. The 20-year means are computed over recent past (a, d) 1981–2000, near future (b, e) 2023–2042, and late 21st century (c, f) 2066–2085. Phototrophy onset corresponds to the day that bottom ice PAR reaches the lowest reported light compensation intensity, that is, the threshold for phototrophic growth. Color scales were chosen to allow the comparison of ice and snow thickness in terms of light attenuation, considering that the light attenuation coefficient of snow is approximately 10 times higher than the attenuation coefficient of sea ice, that is, 10 cm of snow attenuates approximately as much as 1 m of ice.

zero to negative values, indicating that nutrients are depleted before high levels of bottom ice PAR are attained. In this case, the negative number of high growth days measures the asynchrony of light and N availability, whether it is the result of low replenishment of nutrients during winter or sufficient light reaching the bottom of the ice only in late spring. In contrast, areas with a positive number of high growth days are restricted to the coasts of the Laptev and Kara seas, Baffin Bay, and the lower latitudes of the CAA as well as the ice edge in the GIN seas and the Bering Strait. In these regions, this diagnostic reveals simultaneous light and N availability, resulting in a period with both high PAR and nutrients and the possibility of high growth rates.

3.2.3. Environmental controls of ice algal blooms

The combined diagnostics of the phototrophic period and the high growth days characterize the impact of both PAR and nutrient limitation factors and can be used to understand the environmental conditions controlling the growth of ice algae and thus the geographical distribution of sympagic blooms. **Figure 7a**, **b** shows the phototrophic period and the number of high growth days for the recent past, with the spring peak in ice algal biomass shown in **Figure 7c**.

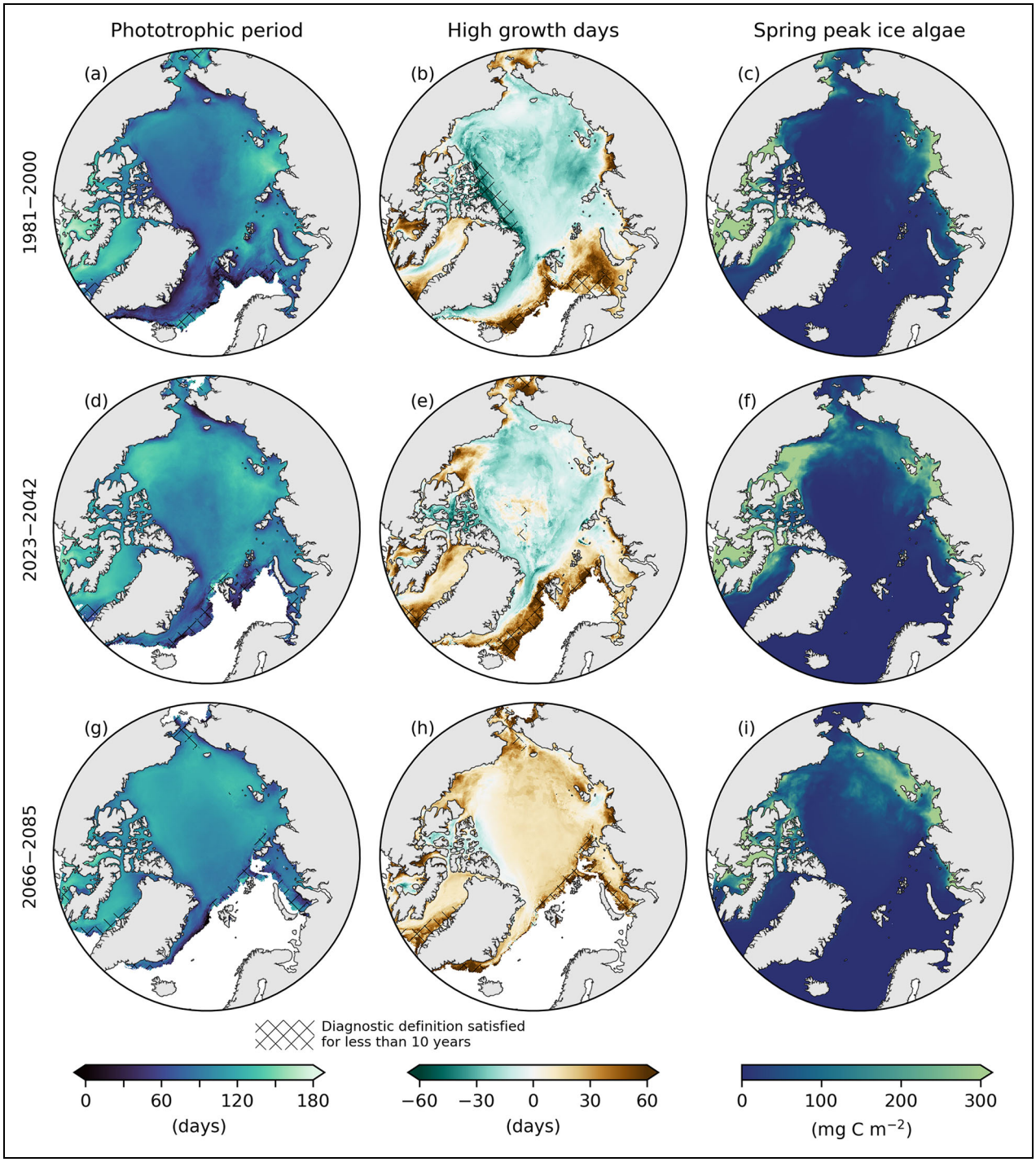

Figure 7. Growth periods and spring peak in ice algae. Climatological growth periods and spring peak in ice algal biomass, for the recent past (a–c), 1981–2000, near future (d–f), 2023–2042, and late 21st century (g–i), 2066–2085. Hatching indicates areas where the diagnostic definition is satisfied for fewer than 10 out of 20 years and for which statistics are less reliable. Diagnostics are described in Section 2.2.

Areas with a positive number of high growth days and a long phototrophic period are those in which some of the most substantial blooms take place. These are the coastal areas of Baffin Bay and the Laptev and Kara seas, as well as the lower latitudes of the CAA, with up to 90 high growth days and simulated ice algae peak biomass in excess of 300 mg C m^{-2}. Note that a positive number of high growth days is not solely sufficient for substantial sympagic growth as demonstrated in the GIN seas which have short phototrophic periods and very little ice algal growth. Indeed, these conditions indicate a potentially fast start to ice algal production due to thin ice allowing high levels of bottom ice PAR as soon as the polar night ends but an abrupt end due to early sea ice break-up, resulting in a period of favorable conditions too short for a large bloom to fully develop.

Non-negligible ice algal blooms can also be found in areas where there are close to zero or even a negative

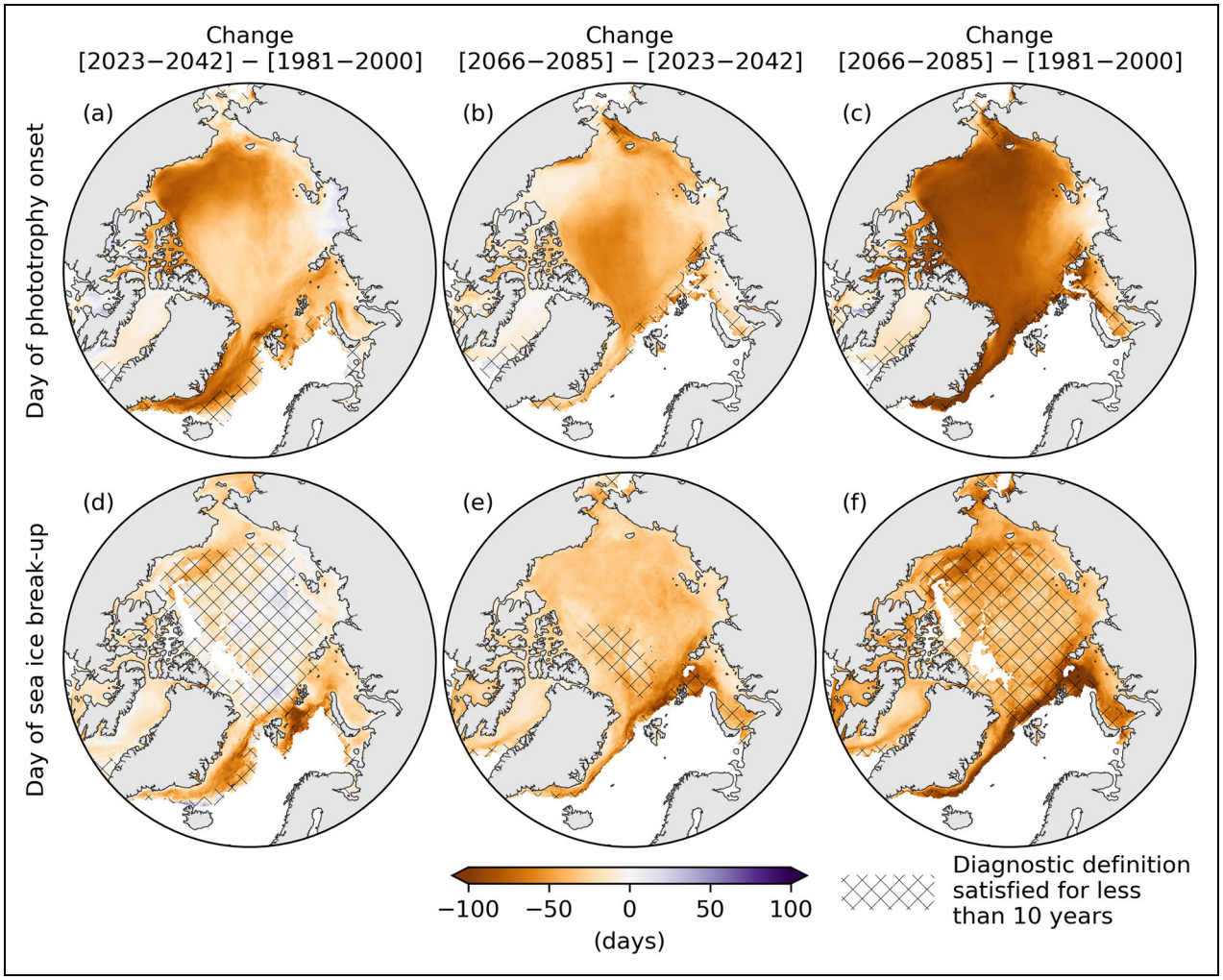

Figure 8. Change in days of phototrophy onset and sea ice break-up. Maps of the change in (a–c) the day of phototrophy onset and (d–f) day of sea ice break-up. Differences in 20-year means are computed over recent past (a, d) 1981–2000, near future (b, e) 2023–2042, and late 21st century (c, f) 2066–2085. Hatching indicates areas where the diagnostic definition is satisfied for less than 10 out of 20 years. Diagnostics are described in Section 2.2.

number of high growth days but only if there is a long phototrophic period. This combination is the case in the Amundsen Gulf, the south of the Beaufort Sea and the north of the Laptev Sea which experience 4–6 months of sufficient light for photosynthesis, and thus, despite the low nutrient levels reached before high levels of light, a long slow bloom develops.

Finally, areas such as the central Arctic with negative numbers of high growth days and a short phototrophic period are strongly growth-limited throughout spring, and therefore harbor almost no ice algae. At the highest latitudes, N limitation occurs even before the onset of phototrophy (**Figure 4a**, **c**), which is a sign of oligotrophy and shows that lack of light is not the only limiting factor in many areas.

3.3. Future changes in ice algal growth

3.3.1. Changes in growth conditions

The diagnostics defined in this work provide a means to assess projected environmental changes that impact ice algae as the Arctic warms in the near future (2023–2042) and by late 21st century (2066–2085).

On the day of phototrophy onset, substantial changes can already be noted in the near future (**Figures 4e**, **n**, **q**, **5e**, **n**, **q**, and **8a**), with the pan-Arctic median date occurring 37 days earlier (Figure S4). By late 21st century, phototrophy starts more than 3 months earlier than during the recent past in a large part of the Arctic (**Figure 8c**). The magnitude and spatial patterns of change in the day of half PAR limitation show similarities to those of the onset of phototrophy, and by late 21st century, high levels of light are projected to reach the bottom of the ice before the end of March in a large part of the Arctic (**Figures 4i**, **5i**, and **9c**). For these two diagnostics, a reduction in spatial variability is seen in both future periods, with a pan-Arctic distribution of phototrophy onset from February to March, and half PAR limitation from February to April, in the period 2066–2085 (Figure S4).

The most substantial shifts in the timing of light availability from the recent past to the near future occur in the Beaufort, Chukchi, and GIN seas, but these areas experience less change during the transition from near future to late 21st century (**Figures 8a**, **b** and **9a**, **b**). Conversely, regions such as the central Arctic and the coast of the East

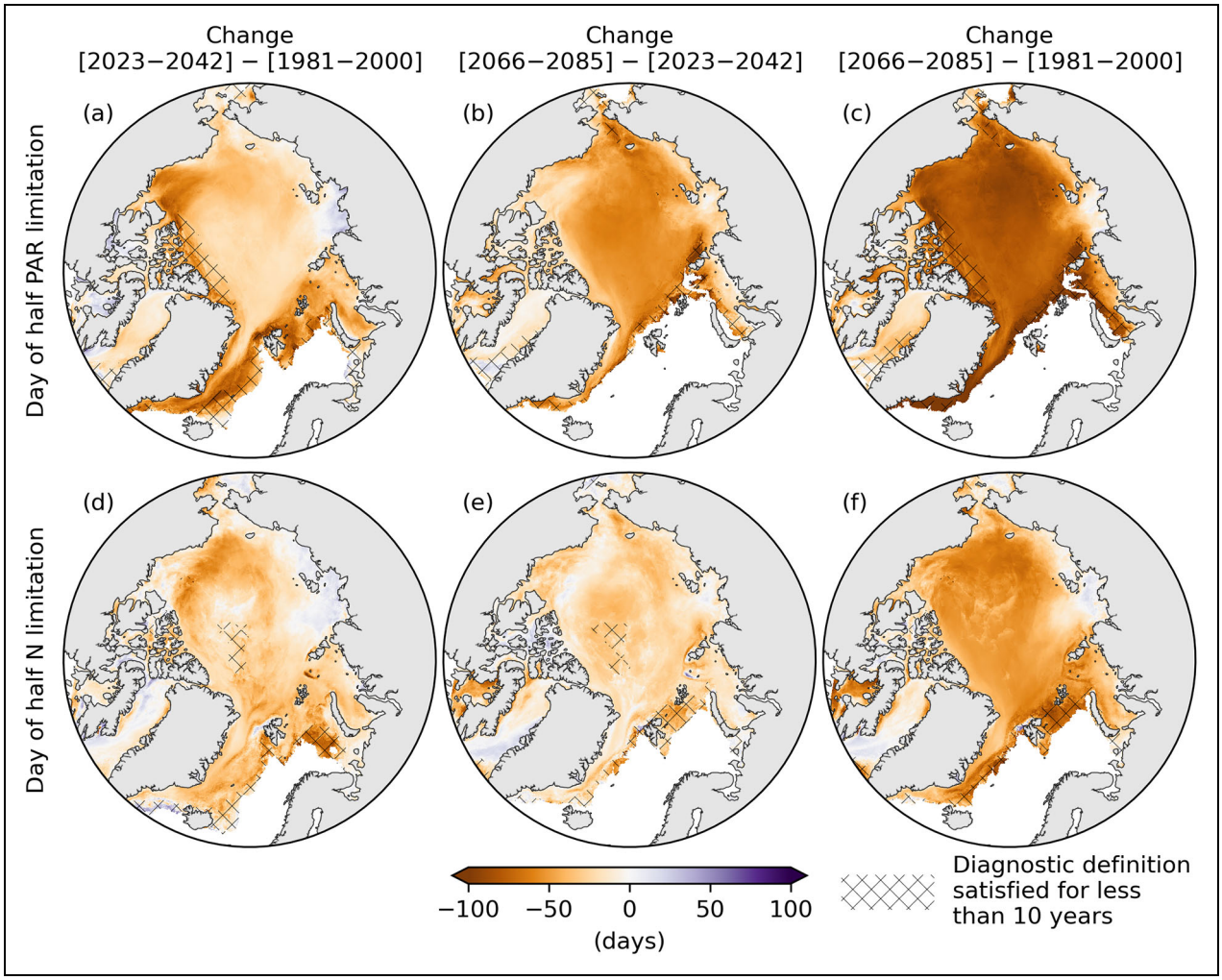

Figure 9. Change in days of half PAR and half N limitation. Maps of the change in (a–c) the day of half PAR limitation and (d–f) day of half N limitation. Differences in 20-year means are computed over recent past (a, d) 1981–2000, near future (b, e) 2023–2042, and late 21st century (c, f) 2066–2085. Hatching indicates areas where the diagnostic definition is satisfied for less than 10 out of 20 years. Diagnostics are described in Section 2.2.

Siberian Sea that see only limited advances from the recent past to the near future, see the most change after the 2023–2042 period.

In both future periods, substantial loss of ice thickness is simulated throughout the Arctic (**Figures 6b**, **c** and S5). In contrast, changes in snow cover are non-monotonic with, at first, a near-future increase in snow thickness on the day of phototrophy onset and of half PAR limitation (**Figure 6e**). This increase is the result of a thicker snow cover throughout spring due to increased total precipitation (Figure S8, Reader and Steiner, 2022). Associated with a substantial shift in the timing of light availability, a thick snow cover indicates that phototrophy onset and half PAR limitation occur before snow begins to melt. From near future to late 21st century, the snow cover is reduced (**Figure 6f**), likely from increased snow to rain conversions and a shorter ice season resulting in less time for the accumulation of snow. These changes indicate that in both future periods the year-round loss of ice thickness is responsible for earlier days of phototrophy onset and of half PAR limitation and that, in the future, snow melt timing has a smaller impact on the timing of light availability in most of the Arctic.

In the Laptev Sea, Baffin Bay and the lower latitudes of the CAA, simulated increases in snow thickness compensate for thinner ice (**Figure 6b**, **c**, **e**, **f**) and result in little change or even delays in the timing of light availability in the future (**Figures 8a**, **b** and **9a**, **b**). As a consequence, by late 21st century, areas of the CAA and the coasts of the East Siberian and Laptev seas are projected to have a later occurrence of half PAR limitation compared to the central Arctic (**Figures 4i** and **5i**).

In the near future, the day of half N limitation is also expected to undergo notable shifts in a large part of the Arctic (**Figures 4g** and **5g**). The most substantial advance is simulated in the basin of the Beaufort Sea and in the Chukchi Sea but also in the GIN and Kara seas, where low levels of nutrients are reached up to 2 months earlier than in the recent past (**Figure 9d**). However, along the continental shelves, the simulated changes are smaller, with the Laptev Sea and the Gulf of Boothia in the CAA showing a later occurrence of half N limitation. This shelf-basin

contrast in projected changes is less pronounced during the transition from near future to late 21st century (**Figure 9e**), and as a result, a smaller spread of the day of half N limitation is simulated over a large part of the Arctic (**Figure 4o**, **r**). This reduced spatial variability is also driven by a reduced spread in the timing of light availability. By late 21st century, nutrient limitation occurs up to 3 months earlier than during the recent past, except in the Laptev Sea and Baffin Bay where simulated changes in the timing of light availability are also limited (**Figure 5o**, **r**).

The day of sea ice break-up shows relatively small changes in the near future compared to the other key dates (**Figures 4h**, **5h**, and **8d**), with a pan-Arctic median only 9 days earlier than the recent past (Figure S4). The shift in sea ice break-up date is projected to accelerate in the transition from near future to late 21st century (Steiner and Reader, 2024), although changes remain comparatively smaller than the shift in the timing of light availability (**Figures 4l**, **5l**, and **8e**). The impact of year-round ice loss is most evident at lower latitudes, in the Bering Strait, GIN, and Barents seas where large changes in break-up date are simulated already in the near future.

3.3.2. Changes in bloom distribution and magnitude

As shown above, the duration of favorable conditions for growth is strongly related to spring peak in ice algae in the recent past, and similarly, changes in timing diagnostics are also linked to the evolution of sympagic blooms in the future. **Figure 7d**–**f** and **g**–**i** shows the phototrophic period, high growth days and spring peak in ice algae for the near future and late 21st century, respectively.

Areas that are projected to experience increases in both the phototrophic period and the number of high growth days also see increases in maximum spring ice algal biomass. In the East Siberian Sea, there is initially only a limited change in timing, mainly in the phototrophic period, which is associated with a minor increase in peak ice algae. However, the increase in periods of favorable growing conditions is amplified from the near future to late 21st century, with a greater area where the number of high growth days exceeds 30 days and the emergence of highly productive areas, in the East Siberian Sea away from the coast.

In the CAA, some areas at higher latitudes that had low productivity in the recent past are expected to develop large blooms during the 21st century. Indeed, the northern regions of the CAA are known to have had some of the thickest ice in the past, but as the ice becomes thinner in a warmer climate, the period of light availability increases substantially. Thus, new hotspots emerge, with large blooms developing in areas of increased high growth days, notably along the coasts of the northern channels of the CAA and in the Gulf of Boothia, which is projected to become one of the most productive areas of the Arctic. Nonetheless, substantial spatial variability is simulated in the CAA, with other non-coastal areas continuing to be growth-limited throughout spring, despite increases in light availability. Similarly, in the central Arctic, the moderate increase of the phototrophic period is not sufficient to support a substantial bloom.

Shortened periods of favorable conditions are associated with reduced ice algal growth, although these combined changes mainly occur in areas that were highly productive in the recent past and which maintain nonetheless significant blooms in the future, such as the lower latitudes of the CAA and of the Laptev Sea. These regions are projected to have decreases in phototrophic period, driven at first by a later day of phototrophy onset in the near future, but then by an earlier sea ice break-up by late 21st century. For these regions, the trend in the number of high growth days is non-monotonic: in the near future, areas where the number of high growth days decreases the most see the biggest change in peak ice algae, but by late 21st century, high growth day numbers increase to past levels. However, for Baffin Bay, the long term decrease in duration of favorable growth conditions is more substantial and leads to the near total loss of ice algal blooms by late 21st century.

Non-monotone responses to climate change are also projected to occur in the Beaufort Sea and the Amundsen Gulf, and to a lesser extent in the Chukchi Sea. At first, in the near future, the period of light availability increases considerably, driven by an earlier onset of phototrophy due to thinner ice. Areas with increases in high growth days become highly productive, reaching some of the highest levels of ice algal biomass. However, as changes in sea ice break-up date become more important, the phototrophic period is substantially reduced, such that, despite positive high growth days, the magnitude of sympagic blooms decreases by late 21st century.

3.4. Ice algae bloom phenology

Figures 10 and **11** show the climatologies of bloom onset and spring peak along with the seasonal cycle of ice algal biomass, for the CAA, Beaufort, East Siberian, and Laptev seas.

3.4.1. Bloom onset

In the recent past, the simulated bloom onset occurs during March and April in most of the Arctic (Figure S9). A notable exception is at lower latitudes, such as in the CAA or the Bering Strait, where blooms begin to develop as early as February. In the Laptev Sea, despite an early beginning of phototrophy, the bloom onset is comparatively late, indicating a slow start attributed to a later day of half PAR limitation (**Figure 11d**).

In the near future, although PAR levels sufficient for phototrophy are reached much earlier than in the recent past, the start of sympagic blooms is not earlier but in fact later, with a pan-Arctic median 9 days later compared to 37 days earlier for phototrophy onset (Figures S4 and S10). Furthermore, the beginning of growth is substantially delayed even in areas where peak ice algae increases are related to changes in timing of light availability, such as the Beaufort and East Siberian seas (**Figures 10e** and **11b**). Bloom onset occurs earlier only in areas where changes in the ice are the most extreme (Figure S9), either at lower latitudes, such as the GIN seas (loss of ice cover),

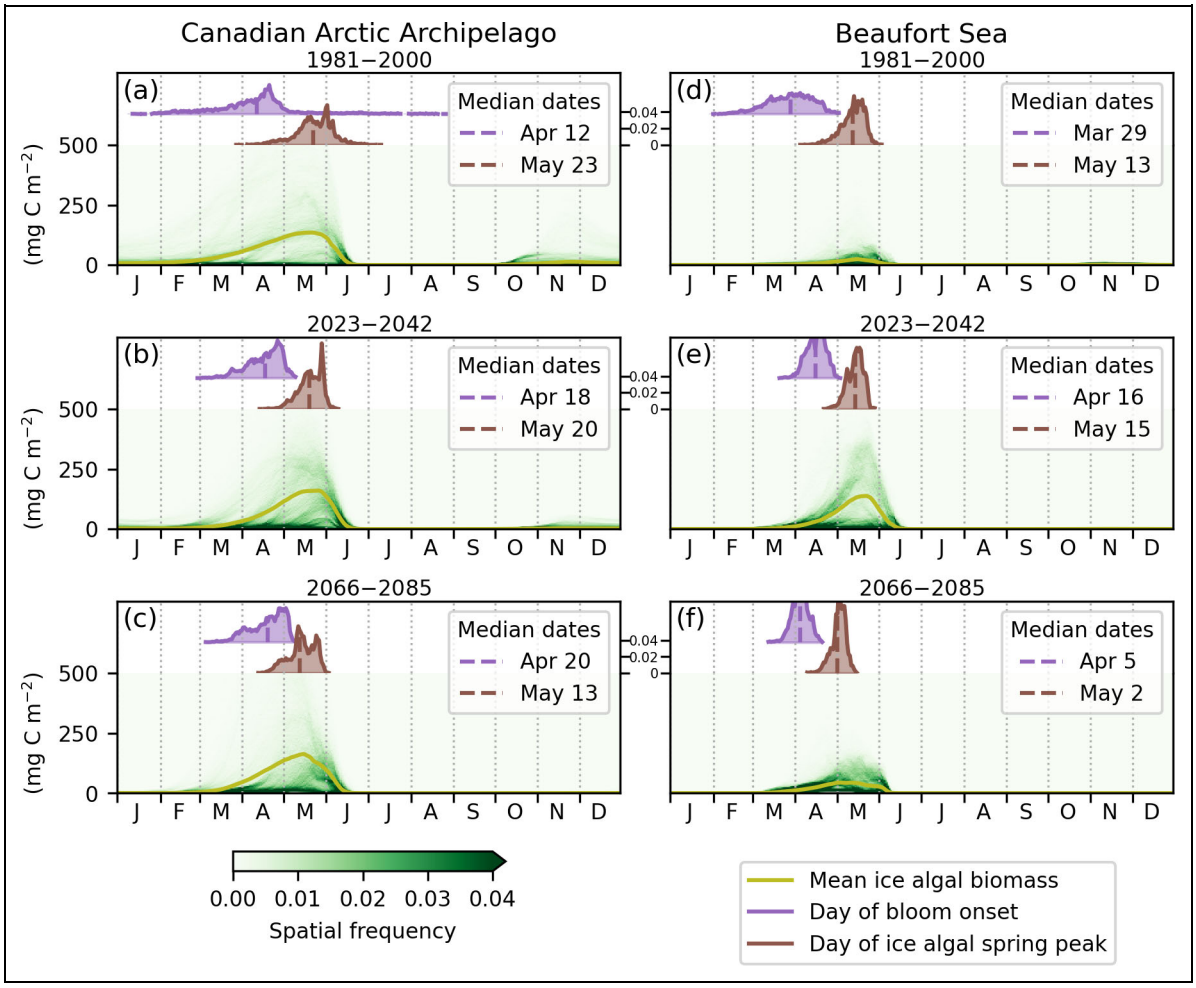

Figure 10. Annual cycle of ice algal biomass for the Canadian Arctic Archipelago and the Beaufort Sea. Annual cycles of regional mean ice algal biomass (mg C m^{-2}) for the Canadian Arctic Archipelago (a–c) and Beaufort Sea (d–f), computed over 20-year periods for the recent past (1981–2000), near future (2023–2042), and late 21st century (2066–2085). To show the spatial spread, the annual cycles of all grid cells in the considered regions are displayed as 2D histograms: the color intensity corresponds to the spatial frequency, that is, the fraction of the region which is at a given ice algal biomass on a given day of the year. Also shown are the histograms of key dates of the bloom for all grid cells within a region: bloom onset (blue) is the day ice algal biomass reaches one standard deviation; and spring peak (red) is the day maximum ice algal biomass is reached, taken before September 1.

or north of Greenland, and the CAA (loss of thick multi-year ice).

By late 21st century, the trend of later bloom onset is reversed and in most of the Arctic, sympagic growth starts slightly earlier than in the near future, but not enough for blooms to happen earlier than in the recent past (**Figures 10c**, **f** and **11c**, **f**). The spread of the bloom onset date is reduced in the future, ranging in a large part of the Arctic from mid-March to late April (Figure S10).

3.4.2. Spring peak

The day when ice algal biomass reaches its annual maximum occurs mostly in May in the recent past (**Figures 10a**, **d** and **11a**, **d**) and generally takes place before the day of half N limitation (**Figures 4m**, **p** and **5m**, **p**). The latest maxima are simulated in the productive areas, such as the Laptev Sea (**Figure 11d**), and the earliest maxima occur in April only in low productivity regions, such as the central Arctic (Figure S11).

Small changes in peak timing are simulated in the near future, with most regions experiencing shifts of less than a few days earlier or later (**Figures 10b**, **e** and **11b**, **e**). By late 21st century, there is a trend toward earlier bloom peaks (**Figures 10c**, **f** and **11c**, **f**), but changes remain small compared to those of other key dates, with a pan-Arctic median only 9 days earlier compared to the recent past (Figure S10). The spread of bloom peaks is reduced in the near future and late 21st century, a decrease particularly notable in the Beaufort and East Siberian seas (**Figures 10e**, **f** and **11b**, **c**).

Both the ice algal bloom phenology diagnostics of bloom onset and spring peak show different spatial patterns than bloom magnitude or timing of light and nutrient availability. Furthermore, the timing of bloom onset and peak indicate that most sympagic activity happens in April and May, with limited change projected in the future. This lack of similarity in both spatial patterns and future changes suggests that, in model simulations, there

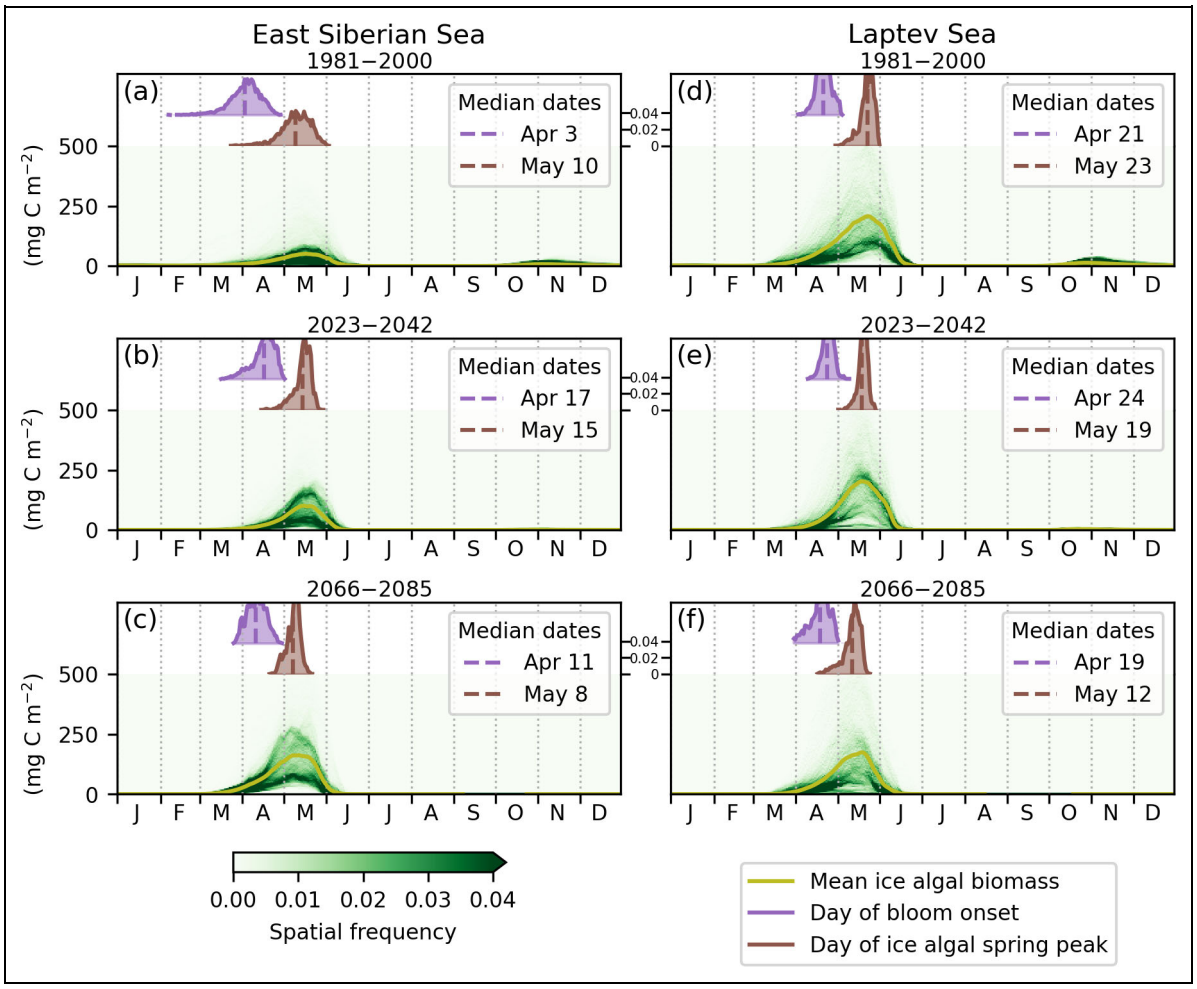

Figure 11. Annual cycle of ice algal biomass for the East Siberian and Laptev seas. Annual cycles of regional mean ice algal biomass (mg C m^{-2}) for the East Siberian (a–c) and Laptev seas (d–f), computed over 20-year periods for the recent past (1988–2000), near future (2023–2042), and late 21st century (2066–2085). To show the spatial spread, the annual cycles of all grid cells in the considered regions are displayed as 2D histograms: the color intensity corresponds to the spatial frequency, that is, the fraction of the region which is at a given ice algal biomass on a given day of the year. Also shown are the histograms of key dates of the bloom for all grid cells within a region: bloom onset (blue) is the day ice algal biomass reaches one standard deviation; and spring peak (red) is the day maximum ice algal biomass is reached, taken before September 1.

is little relationship between the phenology diagnostics and bloom magnitude or limiting factors.

3.4.3. Fall and overwintering ice algae

During fall, as surface nutrients are replenished from enhanced wind mixing, a second phytoplankton bloom can occur (Ardyna et al., 2014). With sea ice growth, phytoplankton can be entrained in newly formed ice and grow while light is still available. In the recent past, starting in October, ice algae accumulate on the bottom of the ice throughout the lower latitudes of the Arctic, reaching 10 mg C m^{-2} in most continental shelf areas and up to 100 mg C m^{-2} in the CAA (**Figure 12a**). However, in the near future, simulated fall ice algae are strongly reduced in most areas, and by late 21st century there are almost no ice algae by the end of the year and the onset of the polar night (**Figure 12b**, **c**). This loss can be attributed to the substantial changes in freeze-up date, with the growth of sea ice starting on continental shelves in mid-to late November in the near future and after December 1 by late 21st century (Figure S12). A delay in ice formation causes a mismatch between the growth of sea ice and the presence of a sufficient quantity of phytoplankton in seawater, as the phytoplankton concentration is strongly reduced by November. Moreover, a later freeze-up reduces the time period when there is sufficient light for algal growth within the ice during fall.

The direct consequence of this loss of fall ice algae is the substantial reduction of overwintering biomass in the future, thereby strongly reducing the initial algal population at the start of spring. The ice algal biomass on the day of phototrophy onset (**Figure 12d**–**f**) provides a means of measuring the starting biomass of the spring bloom that allows meaningful comparisons between the different periods, as opposed to using a fixed date, which would be impacted by changes in light availability. In the recent past, although the starting spring population is reduced compared to the fall, there is non-negligible biomass in

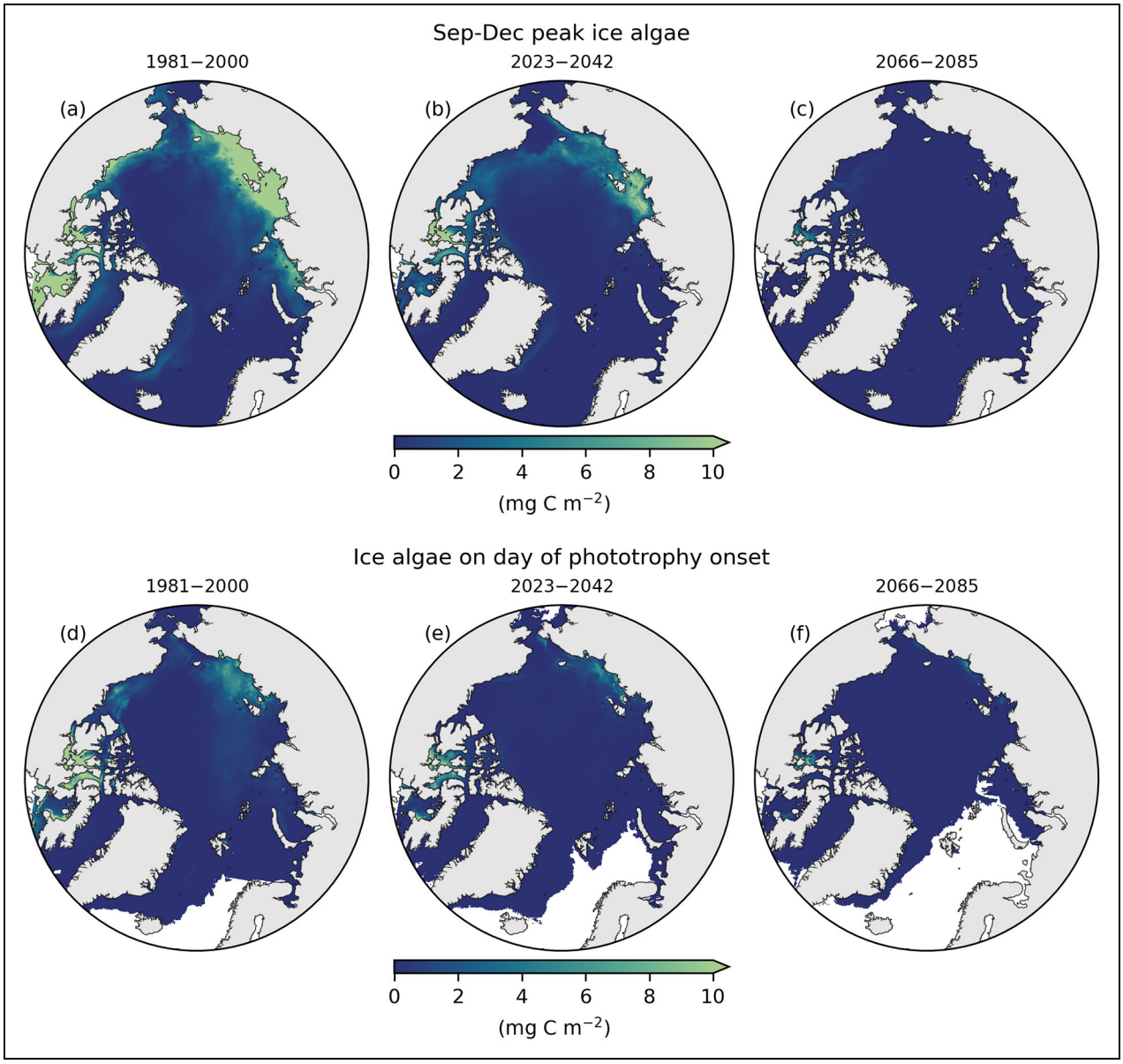

Figure 12. Fall peak ice algae and ice algal biomass on day of phototrophy onset. Top (a–c): maximum ice algal biomass from September 1 to December 31. Bottom (d–f): ice algal biomass on day of phototrophy onset, which is defined as the day that bottom ice photosynthetically active radiation reaches the lowest reported light compensation intensity, that is, the threshold for phototrophic growth. The 20-year means are computed over recent past (1981–2000), near future (2023–2042), and late 21st century (2066–2085).

most of the areas that are productive in spring. However, in the near future and late 21st century, ice algae at the start of spring are strongly reduced, corresponding to the reduced fall ice algae.

4. Discussion

4.1. Environmental controls of ice algal blooms

Substantial differences in the magnitude of sympagic blooms are evident among and within the different regions of the Arctic in the model simulations, as has been found in observations (Leu et al., 2015; Lannuzel et al., 2020) and previous modeling studies (Watanabe et al., 2019). As a consequence, Arctic and even regional averages hide important spatial variability, and interpreting pan-Arctic trends of past and future sea ice ecosystems is difficult. The simulated differences can be attributed to the variety of environmental controls that drive ice algal growth, including a range of different sea ice conditions resulting from complex interactions between a variety of factors such as ocean circulation, continental influences, and bathymetry (Watanabe et al., 2019; Lannuzel et al., 2020).

Models are capable of reproducing the current trends of sea ice loss reasonably well (Hayashida et al., 2019; Crawford et al., 2021), but important uncertainties remain regarding the future of the Arctic environment and the response of sea ice ecosystems (Lannuzel et al., 2020). Although ice algal models have been shown to agree with observations (Mortenson et al., 2017), there are still many uncertainties with respect to ice algal parametrizations

(Steiner et al., 2016). The comparison of model and remote sensing data presented here shows that simulations reproduce the observed large-scale spatial patterns of sea ice break-up timing, albeit with differences in the precise location and timing of sea ice retreat. This evaluation suggests that the model successfully simulates the main features of the sea ice annual cycle, and justifies the use of this model to analyze the processes and mechanisms controlling sympagic growth on a large scale. The main concern of this work is to understand how and why ice algal blooms occur, and thus the precise location and timing of simulated events is less relevant, which mitigates the importance of model biases. The developed timing diagnostics focus on the relationship between environmental conditions and growth rates and are designed to help better understand model behavior. These metrics could be used in future studies to identify precisely why different models produce contrasting results or differ from observations.

The links between the growth period and the magnitude of sympagic blooms that have been shown here emphasize the role of the timing of environmental conditions as a control of ice algal growth. Indeed, the maximum biomass reached during spring depends not only on the growth rates achieved but also on the total length of time available for growth. Importantly, the PAR and N limitation factors used in the model are saturating functions. These factors represent well established properties of algal growth: beyond certain thresholds, additional light or nutrients do not translate into higher growth rates. In addition, because the formulation of the growth rate depends on the minimum of limitation factors, high growth rates are reached only when both PAR and N are sufficient, which highlights the importance of the synchrony of light and N availability. In particular, the timing of bottom ice PAR is highly relevant: earlier high light levels allow for high growth rates before nutrients are depleted. In contrast, if low light persists late into spring, nutrients could be consumed before enough PAR reaches the bottom of the ice for high growth rates. Furthermore, more nutrients at the beginning of spring do not lead directly to higher growth rates, but instead result in a longer period of non-N-limited growth, allowing time for PAR to increase sufficiently such that there can be a period of both high light and nutrients.

Thus, with a focus only on light availability, the phototrophic period alone is not an adequate diagnostic to explain the spatial distribution of sympagic blooms and their magnitude. As regions with short phototrophic periods see little growth, a long phototrophic period is a necessary but not sufficient condition for a strong bloom. The correspondence of the number of high growth days and the spring peak ice algal biomass highlights the necessity to account for both limiting factors in order to understand ice algal blooms. This perspective emphasizes the role of nutrient availability in shaping the spatial distribution of sympagic blooms, as suggested from observations (Rózańska et al., 2009; Lannuzel et al., 2020; Campbell et al., 2022a). The representation of the balance of light and nutrients has also been recognized as driving differences in modeled distributions and projections of pelagic blooms in the Arctic (Vancoppenolle et al., 2013). Although modeling studies have found a sensitivity of sympagic productivity to winter nutrient levels (Watanabe et al., 2019; Jeffery et al., 2020), they do not analyze the impact of other processes influencing nutrient availability during spring, such as remineralization or exchanges with surface seawater.

The diagnostics developed here combine in an effective and efficient manner the different factors influencing both light and nutrient availability. With these metrics, our work analyzes and explains the spatial variability of simulated sympagic blooms through the timing of environmental conditions, including not only the influence of light but also nutrients. Previous modeling studies have shown that the length of the sea ice season sets an upper limit on the productivity of sympagic blooms (Tedesco and Vichi, 2014; Selz et al., 2018), but do not examine the impact of nutrient limitation on the length of the growth season. By quantifying the impact of environmental conditions on ice algal growth, these diagnostics help to interpret the simulated future changes to the Arctic environment and how climate change will affect sympagic ecosystems.

4.2. Climate change impacts

Climate change affects the factors controlling ice algal growth differently in the various regions of the Arctic. The loss of sea ice is perhaps the most direct change impacting ice algae, with the decline in ice cover reducing the available surface area of algal habitat. However, the loss of ice cover is expected to occur first in summer. In the simulation analyzed here, before late 21st century, many regions still have ice break-up dates in June and later, after sympagic blooms have peaked. Springtime sea ice changes lead to a near total loss of ice algae before 2085 only at locations in lower latitudes, in particular in the Bering Strait and the southern Chukchi Sea, or regions of lower past productivity, such as the Barents and GIN seas. Similarly, in the only other model study of future ice algae, decreases in spatially integrated gross primary production in sea ice due to loss of the ice only occur below 60°N (Tedesco et al., 2019). Nonetheless, the expectation is that sea ice loss will eventually become detrimental to ice algae throughout the Arctic (Lannuzel et al., 2020). Our results show that indeed, by the late 21st century, earlier sea ice break-up will start to impact negatively the length of the growing season, with consequences on the spring peak in ice algae, as seen in the Beaufort Sea.

The simulation presented here ends in 2085. At later times, more regions could be impacted by sea ice loss, in particular considering results from CMIP6 Earth System Models, which expect less than 3 months of ice cover in most of the Arctic by 2100, for the scenario with the most warming (Crawford et al., 2021).

At higher latitudes the effects of reductions of ice thickness dominate in the simulations studied here as well as in other model projections of future sympagic blooms (Tedesco et al., 2019). With year round thinner ice, substantial increases of bottom ice PAR are projected to occur,

in particular during the early spring months, with most regions of the Arctic reaching light levels sufficient for photosynthesis before March in the late 21st century. In contrast, the date of sea ice break-up shows comparatively little to no change, in particular in the near future. Together, these factors lead to longer periods of light availability. This results in the emergence of large blooms at high latitudes, at least transitionally during the near future period, notably in the Beaufort and East Siberian seas. Our work broadly confirms the conclusions of studies based on observations of sea ice thickness decline, which anticipate longer periods of algal growth and increased productivity of sympagic blooms, in the near future at least (Lannuzel et al., 2020; Lim et al., 2022). Long growing seasons are also simulated during the late 21st century at high latitudes, in the East Siberian Sea and the CAA.

However, periods of light availability do not increase everywhere in the model simulation, as greater snow cover compensates for the loss of ice thickness in some regions. Notably, the Laptev Sea or the lower latitudes of the CAA are simulated to have shorter growing seasons that are not related to early sea ice break-up but rather are the result of thicker snow delaying the onset of the phototrophic period. Indeed, snow has a much greater light attenuation coefficient than ice (**Table 1**), and small changes in snow accumulation can have greater consequences for light transmission than the loss of ice (Leu et al., 2015). Moreover, CMIP6 models project greater total precipitation (rainfall plus snowfall) in the Arctic and a continued increase of winter snowfall during the 21st century, albeit with a substantial spread in the projected total precipitation changes among CMIP6 models (Crawford et al., 2021). Importantly, most of the increase in total precipitation during other seasons is expected to result in greater rainfall (Tedesco et al., 2019; Reader and Steiner, 2022). Rain events can accelerate ice melt and the flushing of ice algae (Galindo et al., 2014) which could cause earlier bloom termination in the future. Furthermore, changes in cloud state would not only alter snowfall but also the amount of shortwave and longwave radiation reaching the ice surface. There is a high degree of uncertainty in future changes, as a number of interdependent atmospheric processes could be impacted in a variety of manners by climate change, modifying the energy balance (Reader and Steiner, 2022; Ruman et al., 2022; Miyawaki et al., 2023) or cloud formation from aerosols (Abbatt et al., 2019).

Climate change will also impact ice algae by altering nutrient availability, distribution, and dynamics. In the model simulation, changes in the day when nutrients become limiting for growth are not uniform across the Arctic. Nutrient depletion occurs earlier due to the advance in light availability, which can drive earlier consumption. Changes in the timing of light availability also lead to a better synchrony of high levels of light and nutrients, resulting in higher growth rates and therefore a more rapid exhaustion of nutrients (Duarte et al., 2017). In contrast, bottom ice N can be sustained through remineralization, which is expected to increase from greater heterotrophic activity (Lannuzel et al., 2020).

Nutrient availability in sea ice is constrained by the initial stocks at the end of winter and replenishment during spring from exchanges with surface seawater, both of which could increase or decrease depending on future ocean energetics, stratification, coastal runoff and advective fluxes from other ocean basins. Global models project a decrease in sea surface nitrate in the Arctic during the 21st century, from enhanced stratification due to increased surface freshwater content but also from decreasing nitrate in the inflowing North Atlantic and Pacific waters (Vancoppenolle et al., 2013; Barber et al., 2015). Within sea ice, there are still important uncertainties on nutrient dynamics, as sea ice loss and altered wind forcing could lead to increased mixing (Lannuzel et al., 2020). On the continental shelves, areas where the water column is very shallow are already evenly mixed every winter and thus increases in mixing rates are unlikely to yield large changes in nitrate supply (Barber et al., 2015).

4.3. Future ice algal bloom phenology

The diagnostics of ice algal bloom phenology show that little change in the timing of sympagic blooms is projected by the model, in contrast with the diagnostics of environmental timing which clearly indicate earlier and longer growth periods in most of the Arctic.

Various events can be used to assess bloom phenology, from growth onset to bloom termination. The timing of the spring ice algal peak marks the beginning of the end of the bloom, as by definition it occurs just before biomass begins to decrease. Bloom termination is generally attributed to the flushing of the ice algae once the ice temperature increases and brine drainage becomes important or from ablation due to warm underlying water melting the subsurface of the ice (Leu et al., 2015). While an alternative cause to a decrease in ice algae could be nutrient depletion, with the current model parametrization (**Table 1**), to achieve higher mortality than growth, the nutrient limitation factor must be less than 0.05. This value represents a growth rate less than 5% of the maximum achievable, which corresponds to extremely low levels of nutrients. Moreover, in the simulation studied here, the onset of nutrient limitation occurs after the ice algal maximum in productive regions, and therefore nutrients seem to play only a small role in the termination of ice algal blooms.

Shifts in the timing of the spring peak are therefore more indicative of changes in the physical processes controlling ice melt. Thus, the absence of substantial future changes in the timing of the ice algal maximum in the model simulation is the result of limited changes in the onset of ice melt, as seen in the trends of sea ice break-up. By the late 21st century, the ice algae spring peak begins to occur earlier in the year. As previously discussed, changes in the timing of ice melt could be more important after the period considered here, resulting in a much earlier ice algal biomass maximum.

Despite earlier levels of light sufficient for photosynthesis in the future, there is almost no shift in the timing of bloom onset throughout the Arctic in the model simulation. This outcome can be explained by the lower levels

of biomass at the onset of phototrophy in the future, because in the model, the initial ice algal biomass in spring plays an important role in the timing of the bloom. Indeed, the impact on bloom development was shown with the 1D version of model used here (Mortenson et al., 2017) and in another 1D model of landfast ice (Jin et al., 2006). The strong sensitivity to initial biomass in the model can be related to the growth rate formulation, which depends linearly on biomass (Equation 1). Neglecting quadratic mortality and transport (which is reasonable during the initial growth phase), the ice algal model reduces to a linear differential equation, the solution of which is exponential growth. Such a parametrization is commonly used in models, as it is based on observations and is well suited to reproduce the main growth phase of blooms. However, this formulation can lead to very slow growth at first when biomass is low, particularly if strong light limitation results in long doubling times. For example, at bottom ice PAR levels corresponding to phototrophy onset and neglecting transport and mortality terms, the doubling time of ice algal biomass with the current model parameters is 35 days. A halving of the biomass at the beginning of spring in the future would compensate for more than a month of advance of the phototrophy onset date. Therefore, the strong decrease in initial ice algal biomass projected by the model in the future delays the spring blooms, and offsets the direct effect of earlier bottom ice PAR.

The substantial reduction of the initial spring biomass from the near future to late 21st century mirrors the simulated decrease in fall ice algal biomass. Observations have documented high levels of biomass in the fall, albeit with substantial variability (Juterzenka and Knickmeier, 1999). Studies conducted during the autumnal freeze-up have examined how algal populations are first established during ice formation (Garrison et al., 1989; Riedel et al., 2007). Although it has been recognized that some in situ growth can occur (van Leeuwe et al., 2018), the entrainment of organisms from seawater during freezing is found to be the more important process (Gradinger and Ikävalko, 1998; Juterzenka and Knickmeier, 1999).

Seeding mechanisms of ice algal blooms remain unclear, but it has been hypothesized that initial spring ice algal populations originate in the fall and that selection processes occurring during ice formation could play a role in shaping the initial community assemblages of early spring (Tuschling et al., 2000; Riedel et al., 2007; Rózańska et al., 2008; van Leeuwe et al., 2018). The link from fall to spring in terms of biomass quantities has received little attention, but Niemi et al. (2011) observed that during winter, a higher abundance of ice algae was found in the ice that had formed the earliest. This finding could be explained by higher concentrations of protists in seawater that can be incorporated in sea ice at the beginning of fall. As a consequence, the timing of ice formation has been recognized as having an impact on algal abundance in new ice. Leu et al. (2015) have hypothesized that a later freeze-up in the future would lead to less accumulation of algae during ice growth, resulting in lower overwintering biomass that could delay the development of the spring bloom. To the best of our knowledge, however, no study has shown a direct impact of fall biomass levels on the onset of the spring bloom.

Different explanations for the seeding of ice algal blooms have been proposed, such as initiation from resting spores, produced at the end of the previous bloom, and which remain at stable concentrations in sea ice and seawater throughout winter, or the propagation of ice algae from multiyear ice during early spring (Werner et al., 2007; Olsen et al., 2017). The initial ice algal biomass resulting from such seeding mechanisms can be expected to be independent of the timing of ice formation. If these mechanisms are dominant, the later freeze-up would have less impact on the timing of bloom onset.

Observation-based studies and synthesis reviews in general predict that both onset and termination of blooms will occur earlier in the future, as they focus on the changes in timing of light availability or of sea ice break-up (Campbell et al., 2018; van Leeuwe et al., 2018; Lannuzel et al., 2020; Campbell et al., 2022b). Recently, Hill et al. (2022) monitored two sites with different snow covers in the Chukchi Sea, starting in early spring. They noted that at the site with less snow, not only did bottom ice PAR increase earlier but the ice algal spring bloom developed earlier and lasted longer.

In contrast, not all modelling studies conclude that future blooms will occur earlier in the year. Focusing on trends during the recent past, Selz et al. (2018) concluded that sympagic growth will start and end earlier due to shifts in the onset of light availability and ice melt, whereas Ji et al. (2013) find a weak impact of ice retreat on the timing of the ice algal blooms. Moreover, the recent inter-comparison of 5 ice algal models, which included the model used here, found both positive and negative trends over the period 1980–2009 for the spring peak, ranging from $+1.3$ to -9.7 days per decade for the Canada Basin, for example (Watanabe et al., 2019). In contrast, the only study considering future projections found earlier ice algal blooms at all latitudes at the end of the 21st century (Tedesco et al., 2019).

The simulations presented here demonstrate that the initial ice algal biomass at the beginning of spring is potentially critical for the onset of sympagic blooms. As few studies have been conducted in early spring on the onset of ice algal growth, confirming the relative importance of initial biomass, compared to other factors such as environmental conditions, is difficult. More observations of the onset of sympagic blooms during early spring are needed, as well as improved understanding of the link with fall uptake and overwintering biomass to confirm these model results. In parallel, alternative model approaches for ice algal entrainment into ice during its formation, algal overwintering and the initial phase of ice algal growth should be developed and tested.

4.4. Limitations and uncertainties

Models remain a simple representation of sympagic ecosystems. The model evaluated here includes only a single ice algal component that does not account for the diversity of the microbial communities that inhabit sea ice. In

particular, shifts in community composition that have been observed to occur during the development of blooms and the associated changes in growth characteristics, such as from low to high-light adapted species, are not represented (Campbell et al., 2018; van Leeuwe et al., 2018). A single set of parameters is used to represent ice algae throughout the Arctic, with no regional differences in the modeled ice algae. Moreover, grazers are only represented indirectly, with a constant grazing rate (considered to be included in the linear mortality term), and therefore the model would not capture ecological impacts of earlier algal blooms, such as a potential phenological mismatch between primary producers and consumers (Post, 2017). The importance of fall ice algal biomass to the subsequent spring bloom that we have demonstrated implies that our results are likely quantitatively sensitive to the details of the parametrization of ice algal growth.

Concerning the physical model, an important limitation is the lack of tides in the ocean model, which could have regional impacts on mixing and nutrient fluxes at sea ice–ocean interface. In addition, the sea ice model used here, LIM2, does not have sub-grid ice or snow thickness parametrization, thereby limiting the accuracy of light and heat flux variability, which has been shown to have a strong impact on the simulation of ice algal blooms (Abraham et al., 2015).

Finally, due to the internal variability of climate models, details of spatial patterns or the temporal occurrence of certain events identified here could be simulation-dependent. The use of a single ocean model driven by output from a single atmospheric model is another factor contributing to this simulation dependence. To address this issue, the results of this study should be assessed within multimodel intercomparisons such as the Ice Algae Model Intercomparison project 1 (IAMIP; Watanabe et al., 2019) and IAMIP2, which is currently in progress (Hayashida et al., 2021).

5. Conclusions

Using daily data output from a regional ocean and sea ice model with biogeochemistry, diagnostics have been proposed to assess the phenology of ice algae and the timing of environmental controls of sympagic growth. These metrics have been used in particular to understand the spatial variations of ice algal blooms and the future impacts of climate change on sympagic ecosystems in the Arctic. The main results of this study are the following:

1. The timing of environmental conditions controls ice algal growth. In particular the synchrony of light and nutrient availability determines the magnitude of sympagic blooms.
2. At higher latitudes, loss of thick ice and limited changes in the timing of sea ice break-up in the near future will lead to longer periods of favorable growth conditions, resulting in the emergence of new productive regions.
3. Reduction of ice extent will have a small impact on ice algae before late 21st century, mainly at lower latitudes, but will nonetheless limit the increases of the growing season and thus of sympagic blooms.
4. The timing of the ice algal spring peak shows almost no change in the near future and only a small advance by late 21st century due to limited changes in the date of sea ice break-up, before 2085.
5. Later freeze-up will limit the accumulation of ice algae during ice formation in the fall, leading to lower initial biomass at the beginning of spring, which would potentially delay the development of the spring bloom. Hence, the onset of ice algal growth is not expected to occur earlier in the future, despite earlier light availability due to thinner ice.

Data accessibility statement

The model code and the configuration used for model simulations are archived in the repository (Hayashida 2020) (https://zenodo.org/doi/10.5281/zenodo.3697355). Model output is hosted on Digital Research Alliance of Canada infrastructures and can be made available upon request. Scripts for the analysis of model output is archived in the repository (Haddon 2023) (https://zenodo.org/doi/10.5281/zenodo.10045060). The historical forcing dataset DFS5.2 is available at https://www.drakkar-ocean.eu/. The ORAS4 dataset is available at https://www.cen.uni-hamburg.de/icdc/data/ocean/easy-init-ocean/ecmwf-ocean-reanalysis-system-4-oras4.html. Remote sensing sea ice concentration datasets are available at https://doi.pangaea.de/10.1594/PANGAEA.919777 (AMSR-E ASI, Melsheimer and Spreen, 2020) and https://doi.pangaea.de/10.1594/PANGAEA.898399 (AMSR2 ASI, Melsheimer and Spreen, 2019).

Supplemental files

The supplemental files for this article can be found as follows:

This research includes supplementary material that has been uploaded separately to this document.

Text S1. Comparison of phenology diagnostics computed from biomass and NPP.

Figure S1. Map of day of bloom onset computed from NPP.

Figure S2. Map of day of ice algae maximum computed from NPP.

Figure S3. Comparison of histograms of phenology diagnostics computed from biomass and NPP.

Figure S4. Pan Arctic histograms of key dates.

Figure S5. Map of day of phototrophy onset and day of sea ice break-up.

Figure S6. Map of day of half PAR limitation and day of half N limitation.

Figure S7. Map of ice and snow thickness on day of half PAR limitation.

Figure S8. Map of spring mean ice and snow thickness.

Figure S9. Map of day of bloom onset.

Figure S10. Pan Arctic histograms of bloom onset and peak.

Figure S11. Map of day of ice algae maximum.

Figure S12. Map of sea ice freeze-up date.

Acknowledgments

The authors acknowledge constructive discussions within the Institute of Ocean Sciences and Canadian Center for Climate Modelling and Analysis biogeochemical modelling working group. This research was enabled in part by support provided by BC DRI Group and the Digital Research Alliance of Canada (https://alliancecan.ca).

Funding

This project has received funding from the National Science and Engineering Council New Frontiers in Research Fund (NSERC-NFRFG-2020-00451) in association with the European Union's Horizon 2020 research and innovation program under grant agreement No. 101003826 via project CRiceS (Climate relevant interactions and feedbacks: the key role of sea ice and snow in the polar and global climate system). NS and TS acknowledge funding through Fisheries and Ocean Canada, PF through the NSERC discovery grant. This work contributes to the science plan of Biogeochemical Exchange Processes at Sea Ice Interfaces (BEPSII) and the Surface Ocean-Lower Atmosphere Study (SOLAS), which is partially supported by the U.S. National Science Foundation (Grant OCE-1840868) via the Scientific Committee on Oceanic Research (SCOR).

Competing interests

Authors have no competing interests to declare.

Author contributions

- Substantial contributions to conception and design: AH, AHM, NS.
- Acquisition of data: AH, PF, TS.
- Analysis and interpretation of data: AH, PF, AHM, NS.
- Drafting the article or revising it critically for important intellectual content: All authors.
- Final approval of the version to be published: All authors.

References

Abbatt, JPD, **Leaitch, WR**, **Aliabadi, AA**, **Bertram, AK**, **Blanchet, JP**, **Boivin-Rioux, A**, **Bozem, H**, **Burkart, J**, **Chang, RYW**, **Charette, J**, **Chaubey, JP**, **Christensen, RJ**, **Cirisan, A**, **Collins, DB**, **Croft, B**, **Dionne, J**, **Evans, GJ**, **Fletcher, CG**, **Galí, M**, **Ghahreman, R**, **Girard, E**, **Gong, W**, **Gosselin, M**, **Gourdal, M**, **Hanna, SJ**, **Hayashida, H**, **Herber, AB**, **Hesaraki, S**, **Hoor, P**, **Huang, L**, **Hussherr, R**, **Irish, VE**, **Keita, SA**, **Kodros, JK**, **Köllner, F**, **Kolonjari, F**, **Kunkel, D**, **Ladino, LA**, **Law, K**, **Levasseur, M**, **Libois, Q**, **Liggio, J**, **Lizotte, M**, **Macdonald, KM**, **Mahmood, R**, **Martin, RV**, **Mason, RH**, **Miller, LA**, **Moravek, A**, **Mortenson, E**, **Mungall, EL**, **Murphy, JG**, **Namazi, M**, **Norman, AL**, **O'Neill, NT**, **Pierce, JR**, **Russell, LM**, **Schneider, J**, **Schulz, H**, **Sharma, S**, **Si, M**, **Staebler, RM**, **Steiner, NS**, **Thomas, JL**, **von Salzen, K**, **Wentzell, JJB**, **Willis, MD**, **Wentworth, GR**, **Xu, JW**, **Yakobi-Hancock, JD**. 2019. Overview paper: New insights into aerosol and climate in the Arctic. *Atmospheric Chemistry and Physics* **19**(4): 2527–2560. DOI: http://dx.doi.org/10.5194/acp-19-2527-2019.

Abraham, C, **Steiner, N**, **Monahan, A**, **Michel, C.** 2015. Effects of subgrid-scale snow thickness variability on radiative transfer in sea ice. *Journal of Geophysical Research: Oceans* **120**(8): 5597–5614. DOI: http://dx.doi.org/10.1002/2015JC010741.

Ardyna, M, **Babin, M**, **Gosselin, M**, **Devred, E**, **Rainville, L**, **Tremblay, J-É**. 2014. Recent Arctic Ocean sea ice loss triggers novel fall phytoplankton blooms. *Geophysical Research Letters* **41**(17): 6207–6212. DOI: http://dx.doi.org/10.1002/2014GL061047.

Arora, VK, **Scinocca, JF**, **Boer, GJ**, **Christian, JR**, **Denman, KL**, **Flato, GM**, **Kharin, VV**, **Lee, WG**, **Merryfield, WJ.** 2011. Carbon emission limits required to satisfy future representative concentration pathways of greenhouse gases. *Geophysical Research Letters* **38**(5). DOI: http://dx.doi.org/10.1029/2010GL046270.

Balmaseda, MA, **Mogensen, K**, **Weaver, AT.** 2013. Evaluation of the ECMWF ocean reanalysis system ORAS4. *Quarterly Journal of the Royal Meteorological Society* **139**(674): 1132–1161. DOI: http://dx.doi.org/10.1002/qj.2063.

Barber, DG, **Hop, H**, **Mundy, CJ**, **Else, B**, **Dmitrenko, IA**, **Tremblay, J-É**, **Ehn, JK**, **Assmy, P**, **Daase, M**, **Candlish, LM**, **Rysgaard, S.** 2015. Selected physical, biological and biogeochemical implications of a rapidly changing Arctic Marginal Ice Zone. *Progress in Oceanography* **139**: 122–150. DOI: http://dx.doi.org/10.1016/j.pocean.2015.09.003.

Bouillon, S, **Maqueda, MÁM**, **Legat, V**, **Fichefet, T.** 2009. An elastic–viscous–plastic sea ice model formulated on Arakawa B and C grids. *Ocean Modelling* **27**(3–4): 174–184. DOI: http://dx.doi.org/10.1016/j.ocemod.2009.01.004.

Campbell, K, **Lange, BA**, **Landy, JC**, **Katlein, C**, **Nicolaus, M**, **Anhaus, P**, **Matero, I**, **Gradinger, R**, **Charette, J**, **Duerksen, S**, **Tremblay, P**, **Rysgaard, S**, **Tranter, M**, **Haas, C**, **Michel, C.** 2022a. Net heterotrophy in High Arctic first-year and multi-year spring sea ice. *Elementa: Science of the Anthropocene* **10**(1): 00040. DOI: http://dx.doi.org/10.1525/elementa.2021.00040.

Campbell, K, **Matero, I**, **Bellas, C**, **Turpin-Jelfs, T**, **Anhaus, P**, **Graeve, M**, **Fripiat, F**, **Tranter, M**, **Landy, JC**, **Sanchez-Baracaldo, P**, **Leu, E**, **Katlein, C**, **Mundy, CJ**, **Rysgaard, S**, **Tedesco, L**, **Haas, C**, **Nicolaus, M.** 2022b. Monitoring a changing Arctic: Recent advancements in the study of sea ice microbial communities. *Ambio* **51**(2): 318–332. DOI: http://dx.doi.org/10.1007/s13280-021-01658-z.

Campbell, K, **Mundy, CJ**, **Belzile, C**, **Delaforge, A**, **Rysgaard, S.** 2018. Seasonal dynamics of algal and bacterial communities in Arctic sea ice under variable snow cover. *Polar Biology* **41**(1): 41–58. DOI: http://dx.doi.org/10.1007/s00300-017-2168-2.

Castellani, G, **Losch, M**, **Lange, BA**, **Flores, H.** 2017. Modeling Arctic sea-ice algae: Physical drivers of spatial distribution and algae phenology. *Journal of*

Geophysical Research: Oceans **122**(9): 7466–7487. DOI: http://dx.doi.org/10.1002/2017JC012828.

Christian, JR, **Denman, KL**, **Hayashida, H**, **Holdsworth, AM**, **Lee, WG**, **Riche, OGJ**, **Shao, AE**, **Steiner, N**, **Swart, NC.** 2022. Ocean biogeochemistry in the Canadian earth system model version 5.0.3: CanESM5 and CanESM5-CanOE. *Geoscientific Model Development* **15**(11): 4393–4424. DOI: http://dx.doi.org/10.5194/gmd-15-4393-2022.

Crawford, A, **Stroeve, J**, **Smith, A**, **Jahn, A.** 2021. Arctic open-water periods are projected to lengthen dramatically by 2100. *Communications Earth & Environment* **2**(1): 1–10. DOI: http://dx.doi.org/10.1038/s43247-021-00183-x.

Deal, C, **Jin, M**, **Elliott, S**, **Hunke, E**, **Maltrud, M**, **Jeffery, N.** 2011. Large-scale modeling of primary production and ice algal biomass within Arctic sea ice in 1992. *Journal of Geophysical Research: Oceans* **116**(C7). DOI: http://dx.doi.org/10.1029/2010JC006409.

Duarte, P, **Meyer, A**, **Olsen, LM**, **Kauko, HM**, **Assmy, P**, **Rösel, A**, **Itkin, P**, **Hudson, SR**, **Granskog, MA**, **Gerland, S**, **Sundfjord, A**, **Steen, H**, **Hop, H**, **Cohen, L**, **Peterson, AK**, **Jeffery, N**, **Elliott, SM**, **Hunke, EC**, **Turner, AK.** 2017. Sea ice thermohaline dynamics and biogeochemistry in the Arctic Ocean: Empirical and model results. *Journal of Geophysical Research: Biogeosciences* **122**(7): 1632–1654. DOI: http://dx.doi.org/10.1002/2016JG003660.

Dussin, R, **Barnier, B**, **Brodeau, L**, **Molines, JM.** 2016. Drakkar forcing set DFS5. MyOcean Report 01-04-16. Grenoble, France: LGGE.

Galindo, V, **Levasseur, M**, **Mundy, CJ**, **Gosselin, M**, **Tremblay, J-É**, **Scarratt, M**, **Gratton, Y**, **Papakiriakou, T**, **Poulin, M**, **Lizotte, M.** 2014. Biological and physical processes influencing sea ice, under-ice algae, and dimethylsulfoniopropionate during spring in the Canadian Arctic Archipelago. *Journal of Geophysical Research: Oceans* **119**(6): 3746–3766. DOI: http://dx.doi.org/10.1002/2013JC009497.

Garrison, DL, **Close, AR**, **Reimnitz, E.** 1989. Algae concentrated by frazil ice: Evidence from laboratory experiments and field measurements. *Antarctic Science* **1**(4): 313–316. DOI: http://dx.doi.org/10.1017/S0954102089000477.

Gradinger, R, **Ikävalko, J.** 1998. Organism incorporation into newly forming Arctic sea ice in the Greenland sea. *Journal of Plankton Research* **20**(5): 871–886. DOI: http://dx.doi.org/10.1093/plankt/20.5.871.

Haddon, A. 2023. Scripts for the analysis of CSIB model output: v2023.10.26. DOI: http://dx.doi.org/10.5281/zenodo.10045061.

Hayashida, H. 2020. Model code and output of CSIBv4 pan-Arctic sea ice-ocean DMS simulation. Zenodo. DOI: http://dx.doi.org/10.5281/zenodo.3697356.

Hayashida, H, **Carnat, G**, **Galí, M**, **Monahan, AH**, **Mortenson, E**, **Sou, T**, **Steiner, NS.** 2020. Spatiotemporal variability in modeled bottom ice and sea surface dimethylsulfide concentrations and fluxes in the Arctic during 1979–2015. *Global Biogeochemical Cycles* **34**(10): e2019GB006456. DOI: http://dx.doi.org/10.1029/2019GB006456.

Hayashida, H, **Christian, JR**, **Holdsworth, AM**, **Hu, X**, **Monahan, AH**, **Mortenson, E**, **Myers, PG**, **Riche, OGJ**, **Sou, T**, **Steiner, NS.** 2019. CSIB v1 (Canadian sea-ice biogeochemistry): A sea-ice biogeochemical model for the NEMO community ocean modelling framework. *Geoscientific Model Development* **12**(5): 1965–1990. DOI: http://dx.doi.org/10.5194/gmd-12-1965-2019.

Hayashida, H, **Jin, M**, **Steiner, NS**, **Swart, NC**, **Watanabe, E**, **Fiedler, R**, **Hogg, AM**, **Kiss, AE**, **Matear, RJ**, **Strutton, PG.** 2021. Ice Algae Model Intercomparison Project phase 2 (IAMIP2). *Geoscientific Model Development* **14**(11): 6847–6861. DOI: http://dx.doi.org/10.5194/gmd-14-6847-2021.

Hayashida, H, **Steiner, N**, **Monahan, A**, **Galindo, V**, **Lizotte, M**, **Levasseur, M.** 2017. Implications of sea-ice biogeochemistry for oceanic production and emissions of dimethyl sulfide in the Arctic. *Biogeosciences* **14**(12): 3129–3155. DOI: http://dx.doi.org/10.5194/bg-14-3129-2017.

Hill, V, **Light, B**, **Steele, M**, **Sybrandy, AL.** 2022. Contrasting sea-ice algae blooms in a changing Arctic documented by autonomous drifting buoys. *Journal of Geophysical Research: Oceans* **127**(7): e2021JC017848. DOI: http://dx.doi.org/10.1029/2021JC017848.

Jeffery, N, **Maltrud, ME**, **Hunke, EC**, **Wang, S**, **Wolfe, J**, **Turner, AK**, **Burrows, SM**, **Shi, X**, **Lipscomb, WH**, **Maslowski, W**, **Calvin, KV.** 2020. Investigating controls on sea ice algal production using E3SMv1.1-BGC. *Annals of Glaciology* **61**(82): 51–72. DOI: http://dx.doi.org/10.1017/aog.2020.7.

Ji, R, **Jin, M**, **Varpe, Ø.** 2013. Sea ice phenology and timing of primary production pulses in the Arctic Ocean. *Global Change Biology* **19**(3): 734–741. DOI: http://dx.doi.org/10.1111/gcb.12074.

Jin, M, **Deal, CJ**, **Wang, J**, **Shin, KH**, **Tanaka, N**, **Whitledge, TE**, **Lee, SH**, **Gradinger, RR.** 2006. Controls of the landfast ice–ocean ecosystem offshore barrow, Alaska. *Annals of Glaciology* **44**: 63–72. DOI: http://dx.doi.org/10.3189/172756406781811709.

Juterzenka, K, **Knickmeier, K.** 1999. Chlorophyll a distribution in water column and sea ice during the Laptev Sea freeze-up study in autumn 1995, in Kassens, H, Bauch, HA, Dmitrenko, IA, Eicken, H, Hubberten, HW, Melles, M, Thiede, J, Timokhov, LA eds., *Land-ocean systems in the Siberian Arctic: Dynamics and history.* Berlin, Germany: Springer: 153–160. DOI: http://dx.doi.org/10.1007/978-3-642-60134-7_15.

Lannuzel, D, **Tedesco, L**, **van Leeuwe, M**, **Campbell, K**, **Flores, H**, **Delille, B**, **Miller, L**, **Stefels, J**, **Assmy, P**, **Bowman, J**, **Brown, K**, **Castellani, G**, **Chierici, M**, **Crabeck, O**, **Damm, E**, **Else, B**, **Fransson, A**, **Fripiat, F**, **Geilfus, NX**, **Jacques, C**, **Jones, E**, **Kaartokallio, H**, **Kotovitch, M**, **Meiners, K**, **Moreau, S**, **Nomura, D**, **Peeken, I**, **Rintala, JM**, **Steiner, N**, **Tison, JL**, **Vancoppenolle, M**, **Van der Linden, F**, **Vichi, M**, **Wongpan, P.** 2020. The future of Arctic

sea-ice biogeochemistry and ice-associated ecosystems. *Nature Climate Change* **10**(11): 983–992. DOI: http://dx.doi.org/10.1038/s41558-020-00940-4.

Leu, E, **Mundy, CJ**, **Assmy, P**, **Campbell, K**, **Gabrielsen, TM**, **Gosselin, M**, **Juul-Pedersen, T**, **Gradinger, R.** 2015. Arctic spring awakening—Steering principles behind the phenology of vernal ice algal blooms. *Progress in Oceanography* **139**: 151–170. DOI: http://dx.doi.org/10.1016/j.pocean.2015.07.012.

Lim, SM, **Payne, CM**, **van Dijken, GL**, **Arrigo, KR.** 2022. Increases in Arctic sea ice algal habitat, 1985–2018. *Elementa: Science of the Anthropocene* **10**(1): 00008. DOI: http://dx.doi.org/10.1525/elementa.2022.00008.

Madec, G, **Bourdallé-Badie, R**, **Bouttier, PA**, **Bricaud, C**, **Bruciaferri, D**, **Calvert, D**, **Chanut, J**, **Clementi, E**, **Coward, A**, **Delrosso, D**, **Ethé, C**, **Flavoni, S**, **Graham, T**, **Harle, J**, **Iovino, D**, **Lea, D**, **Lévy, C**, **Lovato, T**, **Martin, N**, **Masson, S**, **Mocavero, S**, **Paul, J**, **Rousset, C**, **Storkey, D**, **Storto, A**, **Vancoppenolle, M.** 2017. NEMO ocean engine. In Notes du Pôle de modélisation de l'Institut Pierre-Simon Laplace (IPSL) (v3.6-patch, Number 27). Zenodo. DOI: http://dx.doi.org/10.5281/zenodo.3248739.

Matrai, PA, **Olson, E**, **Suttles, S**, **Hill, V**, **Codispoti, LA**, **Light, B**, **Steele, M.** 2013. Synthesis of primary production in the Arctic Ocean: I. Surface waters, 1954–2007. *Progress in Oceanography* **110**: 93–106. DOI: http://dx.doi.org/10.1016/j.pocean.2012.11.004.

Melsheimer, C, **Spreen, G.** 2019. AMSR2 ASI sea ice concentration data, Arctic, version 5.4 (NetCDF) (July 2012–December 2019). PANGAEA. DOI: http://dx.doi.org/10.1594/PANGAEA.898399.

Melsheimer, C, **Spreen, G.** 2020. AMSR-E ASI sea ice concentration data, Arctic, version 5.4 (NetCDF) (June 2002–September 2011). PANGAEA. DOI: http://dx.doi.org/10.1594/PANGAEA.919777.

Miyawaki, O, **Shaw, TA**, **Jansen, MF**. 2023. The emergence of a new wintertime Arctic energy balance regime. *Environmental Research: Climate* **2**(3): 031003. DOI: http://dx.doi.org/10.1088/2752-5295/aced63.

Mock, T, **Gradinger, R.** 1999. Determination of Arctic ice algal production with a new *in situ* incubation technique. *Marine Ecology Progress Series* **177**: 15–26. DOI: http://dx.doi.org/10.3354/meps177015.

Mortenson, E, **Hayashida, H**, **Steiner, N**, **Monahan, A**, **Blais, M**, **Gale, MA**, **Galindo, V**, **Gosselin, M**, **Hu, X**, **Lavoie, D**, **Mundy, CJ.** 2017. A model-based analysis of physical and biological controls on ice algal and pelagic primary production in resolute passage. *Elementa: Science of the Anthropocene* **5**: 39. DOI: http://dx.doi.org/10.1525/elementa.229.

Mortenson, E, **Steiner, N**, **Monahan, AH**, **Hayashida, H**, **Sou, T**, **Shao, A.** 2020. Modeled impacts of sea ice exchange processes on Arctic Ocean carbon uptake and acidification (1980–2015). *Journal of Geophysical Research: Oceans* **125**(7): e2019JC015782. DOI: http://dx.doi.org/10.1029/2019JC015782.

Niemi, A, **Michel, C**, **Hille, K**, **Poulin, M.** 2011. Protist assemblages in winter sea ice: Setting the stage for the spring ice algal bloom. *Polar Biology* **34**(12): 1803–1817. DOI: http://dx.doi.org/10.1007/s00300-011-1059-1.

Olsen, LM, **Laney, SR**, **Duarte, P**, **Kauko, HM**, **Fernández-Méndez, M**, **Mundy, CJ**, **Rösel, A**, **Meyer, A**, **Itkin, P**, **Cohen, L**, **Peeken, I**, **Tatarek, A**, **Rózańska-Pluta, M**, **Wiktor, J**, **Taskjelle, T**, **Pavlov, AK**, **Hudson, SR**, **Granskog, MA**, **Hop, H**, **Assmy, P**. 2017. The seeding of ice algal blooms in Arctic pack ice: The multiyear ice seed repository hypothesis. *Journal of Geophysical Research: Biogeosciences* **122**(7): 1529–1548. DOI: http://dx.doi.org/10.1002/2016JG003668.

Owens, WB, **Millard, RC.** 1985. A new algorithm for CTD oxygen calibration. *Journal of Physical Oceanography* **15**(5): 621–631. DOI: http://dx.doi.org/10.1175/1520-0485(1985)015<0621:ANAFCO>2.0.CO;2.

Petrich, C, **Eicken, H.** 2017. Overview of sea ice growth and properties, in Thomas, DN ed., *Sea ice. 3rd ed.* Chichester, UK; Hoboken, NJ: John Wiley & Sons: 1–41. DOI: http://dx.doi.org/10.1002/9781118778371.ch1.

Post, E. 2017. Implications of earlier sea ice melt for phenological cascades in Arctic marine food webs. *Food Webs* **13**: 60–66. DOI: http://dx.doi.org/10.1016/j.fooweb.2016.11.002.

Reader, MC, **Steiner, N.** 2022. Atmospheric trends over the Arctic Ocean in simulations from the Coordinated Regional Downscaling Experiment (CORDEX) and their driving GCMs. *Climate Dynamics* **59**(11): 3401–3426. DOI: http://dx.doi.org/10.1007/s00382-022-06274-5.

Riedel, A, **Michel, C**, **Gosselin, M**, **LeBlanc, B.** 2007. Enrichment of nutrients, exopolymeric substances and microorganisms in newly formed sea ice on the Mackenzie shelf. *Marine Ecology Progress Series* **342**: 55–67. DOI: http://dx.doi.org/10.3354/meps342055.

Rózańska, M, **Gosselin, M**, **Poulin, M**, **Wiktor, JM**, **Michel, C.** 2009. Influence of environmental factors on the development of bottom ice protist communities during the winter–spring transition. *Marine Ecology Progress Series* **386**: 43–59. DOI: http://dx.doi.org/10.3354/meps08092.

Rózańska, M, **Poulin, M**, **Gosselin, M.** 2008. Protist entrapment in newly formed sea ice in the Coastal Arctic Ocean. *Journal of Marine Systems* **74**(3–4): 887–901. DOI: http://dx.doi.org/10.1016/j.jmarsys.2007.11.009.

Ruman, CJ, **Monahan, AH**, **Sushama, L.** 2022. Climatology of Arctic temperature inversions in current and future climates. *Theoretical and Applied Climatology* **150**(1): 121–134. DOI: http://dx.doi.org/10.1007/s00704-022-04147-9.

Selz, V, **Saenz, BT**, **van Dijken, GL**, **Arrigo, KR.** 2018. Drivers of ice algal bloom variability between 1980 and 2015 in the Chukchi Sea. *Journal of Geophysical*

Research: Oceans **123**(10): 7037–7052. DOI: http://dx.doi.org/10.1029/2018JC014123.

Sibert, V, **Zakardjian, B**, **Saucier, F**, **Gosselin, M**, **Starr, M**, **Senneville, S.** 2010. Spatial and temporal variability of ice algal production in a 3D ice–ocean model of the Hudson Bay, Hudson Strait and Foxe Basin system. *Polar Research* **29**(3): 353–378. DOI: http://dx.doi.org/10.3402/polar.v29i3.6084.

Spreen, G, **Kaleschke, L**, **Heygster, G.** 2008. Sea ice remote sensing using AMSR-E 89-GHz channels. *Journal of Geophysical Research: Oceans* **113**(C2). DOI: http://dx.doi.org/10.1029/2005JC003384.

Steiner, N, **Deal, C**, **Lannuzel, D**, **Lavoie, D**, **Massonnet, F**, **Miller, LA**, **Moreau, S**, **Popova, E**, **Stefels, J**, **Tedesco, L.** 2016. What sea-ice biogeochemical modellers need from observers. *Elementa: Science of the Anthropocene* **4**: 000084. DOI: http://dx.doi.org/10.12952/journal.elementa.000084.

Steiner, NS, **Reader, MC.** 2024. Trends and projections in climate-related stressors impacting Arctic marine ecosystems—A CMIP6 model analysis. Preprints. DOI: http://dx.doi.org/10.22541/essoar.170680227.79348011/v1.

Stroeve, J, **Vancoppenolle, M**, **Veyssiere, G**, **Lebrun, M**, **Castellani, G**, **Babin, M**, **Karcher, M**, **Landy, J**, **Liston, GE**, **Wilkinson, J.** 2021. A multi-sensor and modeling approach for mapping light under sea ice during the ice-growth season. *Frontiers in Marine Science* **7**: 592337.

Stroeve, JC, **Serreze, MC**, **Holland, MM**, **Kay, JE**, **Malanik, J**, **Barrett, AP.** 2012. The Arctic's rapidly shrinking sea ice cover: A research synthesis. *Climatic Change* **110**(3): 1005–1027. DOI: http://dx.doi.org/10.1007/s10584-011-0101-1.

Tedesco, L, **Vichi, M.** 2014. Sea ice biogeochemistry: A guide for modellers. *PLoS One* **9**(2): e89217. DOI: http://dx.doi.org/10.1371/journal.pone.0089217.

Tedesco, L, **Vichi, M**, **Scoccimarro, E.** 2019. Sea-ice algal phenology in a warmer Arctic. *Science Advances* **5**(5): eaav4830. DOI: http://dx.doi.org/10.1126/sciadv.aav4830.

Tuschling, K, **Juterzenka, Kv**, **Okolodkov, YB**, **Anoshkin, A.** 2000. Composition and distribution of the pelagic and sympagic algal assemblages in the Laptev Sea during autumnal freeze-up. *Journal of Plankton Research* **22**(5): 843–864. DOI: http://dx.doi.org/10.1093/plankt/22.5.843.

van Leeuwe, MA, **Tedesco, L**, **Arrigo, KR**, **Assmy, P**, **Campbell, K**, **Meiners, KM**, **Rintala, JM**, **Selz, V**, **Thomas, DN**, **Stefels, J.** 2018. Microalgal community structure and primary production in Arctic and Antarctic sea ice: A synthesis. *Elementa: Science of the Anthropocene* **6**: 4. DOI: http://dx.doi.org/10.1525/elementa.267.

van Vuuren, DP, **Edmonds, J**, **Kainuma, M**, **Riahi, K**, **Thomson, A**, **Hibbard, K**, **Hurtt, GC**, **Kram, T**, **Krey, V**, **Lamarque, JF**, **Masui, T**, **Meinshausen, M**, **Nakicenovic, N**, **Smith, SJ**, **Rose, SK.** 2011. The representative concentration pathways: An overview. *Climatic Change* **109**(1): 5–31. DOI: http://dx.doi.org/10.1007/s10584-011-0148-z.

Vancoppenolle, M, **Bopp, L**, **Madec, G**, **Dunne, J**, **Ilyina, T**, **Halloran, PR**, **Steiner, N.** 2013. Future Arctic Ocean primary productivity from CMIP5 simulations: Uncertain outcome, but consistent mechanisms. *Global Biogeochemical Cycles* **27**(3): 605–619.

Watanabe, E, **Jin, M**, **Hayashida, H**, **Zhang, J**, **Steiner, N.** 2019. Multi-model intercomparison of the pan-Arctic ice-algal productivity on seasonal, interannual, and decadal timescales. *Journal of Geophysical Research: Oceans* **124**(12): 9053–9084. DOI: http://dx.doi.org/10.1029/2019JC015100.

Watanabe, E, **Onodera, J**, **Harada, N**, **Aita, MN**, **Ishida, A**, **Kishi, MJ.** 2015. Wind-driven interannual variability of sea ice algal production in the western Arctic Chukchi borderland. *Biogeosciences* **12**(20): 6147–6168. DOI: http://dx.doi.org/10.5194/bg-12-6147-2015.

Weiss, RF. 1970. The solubility of nitrogen, oxygen and argon in water and seawater. *Deep Sea Research and Oceanographic Abstracts* **17**(4): 721–735. DOI: http://dx.doi.org/10.1016/0011-7471(70)90037-9.

Werner, I, **Ikävalko, J**, **Schünemann, H.** 2007. Sea-ice algae in Arctic pack ice during late winter. *Polar Biology* **30**(11): 1493–1504. DOI: http://dx.doi.org/10.1007/s00300-007-0310-2.

Zhuang, J, **Dussin, R**, **Huard, D**, **Bourgault, P**, **Banihirwe, A**, **Raynaud, S**, **Malevich, B**, **Schupfner, M**, **Filipe, Levang, S, Gauthier, C, Jüling, A, Almansi, M, Richard Scott, OZ, Rondeau, G, Rasp, S, Smith, TJ, Stachelek, J, Plough, M, Pierre, Bell, R, Caneill, R, Li, X.** 2023. Pangeo-data/xESMF: v0.8.2. DOI: http://dx.doi.org/10.5281/zenodo.8356796.

How to cite this article: Haddon, A, Farnole, P, Monahan, AH, Sou, T, Steiner, N. 2024. Environmental controls and phenology of sea ice algal growth in a future Arctic. *Elementa: Science of the Anthropocene* 12(1). DOI: https://doi.org/10.1525/elementa.2023.00129

Domain Editor-in-Chief: Jody W. Deming, University of Washington, Seattle, WA, USA

Associate Editor: Kevin R. Arrigo, Department of Earth System Science, Stanford University, Stanford, CA, USA

Knowledge Domain: Ocean Science

Part of an Elementa Special Feature: Insights into Biogeochemical Exchange Processes at Sea Ice Interfaces (BEPSII-2)

Published: May 15, 2024 **Accepted:** March 22, 2024 **Submitted:** November 01, 2023

ELEMENTA Science of the Anthropocene

Elem Sci Anth is a peer-reviewed open access journal published by University of California Press.

OPEN ACCESS